iScience

CellPress
OPEN ACCESS

Article

Preclinical long-term safety of intraspinal transplantation of human dorsal spinal GABA neural progenitor cells

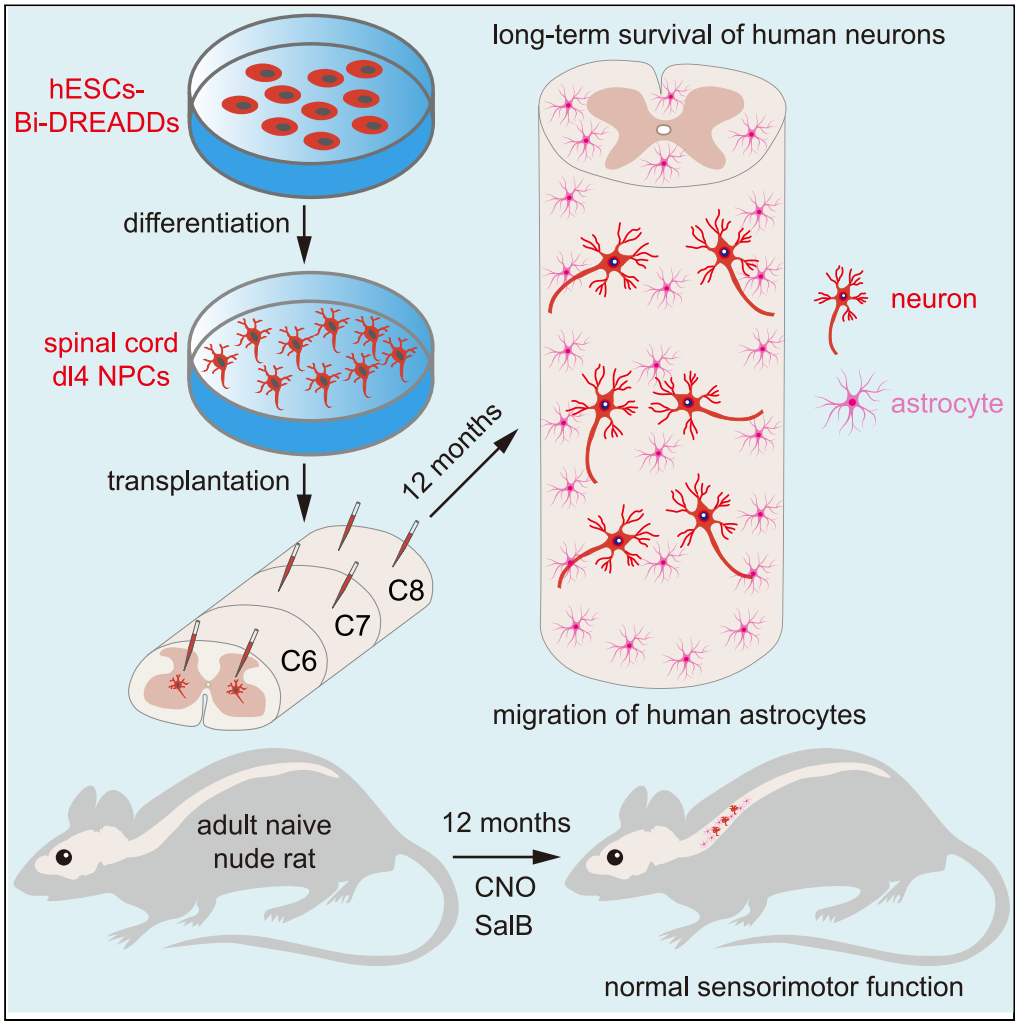

Xiaolong Zheng, Zhixian Liu, Ziyu He, ..., Su-Chun Zhang, Hong Chen, Wei Wang

chenhong1129@hust.edu.cn (H.C.)
wwang@tjh.tjmu.edu.cn (W.W.)

Highlights

Human spinal GABA neurons survive long term and mature in the rat spinal cord

Human spinal GABA neurons integrate into rat neural circuits

Human spinal astrocytes migrate and integrate into the rat spinal cord

Intraspinal transplantation of human spinal NPCs is safe in the long term

Zheng et al., iScience 26, 108306
November 17, 2023
https://doi.org/10.1016/j.isci.2023.108306

iScience

CellPress
OPEN ACCESS

Article

Preclinical long-term safety of intraspinal transplantation of human dorsal spinal GABA neural progenitor cells

Xiaolong Zheng,[1] Zhixian Liu,[1] Ziyu He,[1] Jia Xu,[2,3] YaNan Wang,[2] ChenZi Gong,[2] Ruoying Zhang,[1] Su-Chun Zhang,[4,5] Hong Chen,[2,3,6,*] and Wei Wang[1,6,7,8,*]

SUMMARY

Human pluripotent stem cell (hPSC)-derived neurons have shown promise in treating spinal cord injury (SCI). We previously showed that hPSC-derived dorsal spinal γ-aminobutyric acid (GABA) neurons can alleviate spasticity and promote locomotion in rats with SCI, but their long-term safety remains elusive. Here, we characterized the long-term fate and safety of human dorsal spinal GABA neural progenitor cells (NPCs) in naive rats over one year. All grafted NPCs had undergone differentiation, yielding mainly neurons and astrocytes. Fully mature human neurons grew many axons and formed numerous synapses with rat neural circuits, together with mature human astrocytes that structurally integrated into the rat spinal cord. The sensorimotor function of rats was not impaired by intraspinal transplantation, even when human neurons were activated or inhibited by designer receptors exclusively activated by designer drugs (DREADDs). These findings represent a significant step toward the clinical translation of human spinal neuron transplantation for treating SCI.

INTRODUCTION

Spinal cord injury (SCI) is a devastating disease causing permanent deficits in motor, sensory, and autonomic functions with no effective therapies currently available.[1] Human pluripotent stem cells (hPSCs), including embryonic stem cells (ESCs) and induced pluripotent stem cell (iPSC)-derived neural stem cells (NSCs) or neural progenitor cells (NPCs), which can generate neurons to reconstruct damaged neural circuits, hold great promise in treating SCI[2,] but few have entered into clinical trials.[3–5] Until recently, the first-in-human clinical trial of transplantation of iPSC-derived NSCs or NPCs in subacute complete SCI was initiated.[6] In addition to paralysis, approximately 80% and 65% of SCI patients develop pain[7] and spasm,[8] respectively. These two complications are refractory to drug therapy.[9] Studies on animal models of SCI revealed that loss of spinal inhibitory neurons could be the possible reason for pain and spasm.[10–12] Thus, transplanting human spinal inhibitory neurons might be a candidate therapy for treating pain and spasm in the clinic. All spinal cord neurons are generated from 11 neuronal progenitor domains during embryonic development: pd1–pd6, pV0–pV3. and pMN, which eventually give rise to dI1–dI6, V0–V3, and motor neurons.[13] Sensation is transmitted and regulated by dI1–dI5 neurons,[14] while motor function is coordinated and executed by dI6, V0–V3, and motor neurons.[15] Of note, within dI1–dI5 neurons, only dI4/dIL$_A$ neurons are inhibitory neurons,[16] while dI1–dI3 and dI5/dIL$_B$ neurons are excitatory glutamatergic neurons. Thus, we differentiated human spinal dI4/dIL$_A$ NPCs from human ESCs for transplantation in an attempt to treat pain and spasm after SCI.

We previously showed that hPSC-derived dorsal spinal γ-aminobutyric acid (GABA) neurons can alleviate spasticity and promote locomotion in rats with SCI,[17] and they can survive and integrate into the injured nonhuman primate (NHP) spinal cord,[18] suggesting their potential for treating SCI in the clinic. However, similar to many other SCI studies of hPSC-derived neuron transplantation,[19–22] the observation period of our rat and monkey studies was short, ranging from 3 to 6 months,[17,18] which raises some uncertainty regarding clinical translation. First, for grafted neurons to reconstruct damaged neural circuits, they must permanently survive in the spinal cord of patients, while the life expectancy of SCI patients is many years rather than just a few months.[23] The survival of neurons in a shorter time in animal models (months) does not assure their lifelong survival in patients (years). Second, mounting evidence indicates the very slow maturation of human neurons both

[1]Department of Neurology, Tongji Hospital, Tongji Medical College, Huazhong University of Science and Technology, Wuhan 430030, China
[2]Department of Rehabilitation, Tongji Hospital, Tongji Medical College, Huazhong University of Science and Technology, Wuhan 430030, China
[3]Stem Cell Research Center, Tongji Hospital, Tongji Medical College, Huazhong University of Science and Technology, Wuhan 430030, China
[4]Waisman Center, Department of Neuroscience and Department of Neurology, University of Wisconsin, Madison, WI, USA
[5]Program in Neuroscience & Behavioral Disorders, Duke-NUS Medical School, Singapore, Singapore
[6]Hubei Key Laboratory of Neural Injury and Functional Reconstruction, Huazhong University of Science and Technology, Wuhan 430030, China
[7]Key Laboratory of Neurological Diseases of Chinese Ministry of Education, the School of Basic Medicine, Tongji Medical College, Huazhong University of Science and Technology, Wuhan 430030, China
[8]Lead contact
*Correspondence: chenhong1129@hust.edu.cn (H.C.), wwang@tjh.tjmu.edu.cn (W.W.)
https://doi.org/10.1016/j.isci.2023.108306

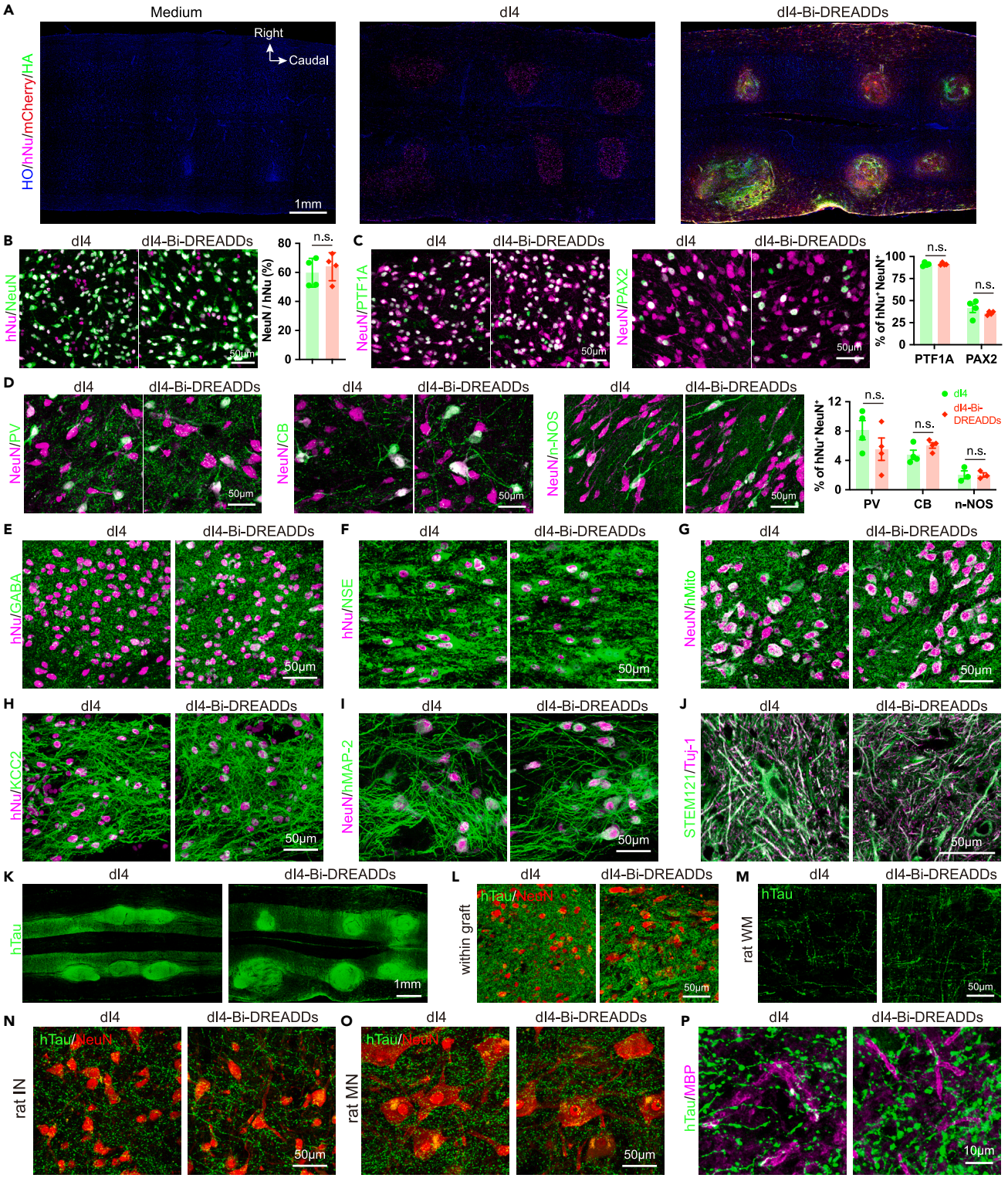

Figure 1. Long-term survival, full maturation and extensive axon growth of human dorsal spinal GABA neurons

(A) Representative images of horizontal sections of adult naive rat C5-C8 spinal cords receiving either human ESC-derived spinal dI4/dIL$_A$ NPCs with or without BiDREADDs expression or cell culture medium, showing long-term survival of grafted cells 12 months post-transplantation.

(B) Images of differentiated human neurons within the graft. Quantifications show the proportions of hNu$^+$NeuN$^+$ human neurons in dI4 (green) and dI4-Bi-DREADDs grafts (red).

Figure 1. *Continued*

(C) Images of human neurons expressing the markers of dI4/dIL$_A$ (PTF1A) and inhibitory interneuron identity (PAX2). Images of hNu were omitted for simplicity. Quantifications show the proportions of PTF1A and PAX2 in dI4 (green) and dI4-Bi-DREADD grafts (red).

(D) Images of human neurons expressing the markers of subtypes of inhibitory neurons. Images of hNu were omitted for simplicity. Quantifications show the proportions of PV, CB and n-NOS in dI4 (green) and dI4-Bi-DREADDs grafts (red).

(E) Images showing that human neurons released much GABA within the graft.

(F–H) Images of the graft showing human neurons extensively expressing NSE (F), hMito (G) and KCC2 (H), suggesting their full maturation.

(I and J) Images of the graft showing that human neurons grew large numbers of hMAP-2$^+$ dendrites (I) and STEM121$^+$Tuj1$^+$ axons (J). STEM121 is a human-specific cytoplasmic marker.

(K–P) Images of hTau$^+$ human axons showing their location, traveling, projection and myelination. Numerous hTau$^+$ human axons existed within the rat C5–C8 spinal cords (K). They were densely intermingled within the graft (L), traveling within the WM (M) and projecting into the GM of rat spinal cords where rat INs (N) and MNs (O) reside. Human axons were unwrapped by an MBP$^+$ myelin sheath (P). Data are represented as the mean ± SEM. n represents number of rats per group. See also Figure S1. Scale bar, 1 mm in (A) and (K), 50 μm in (B–J) and (L–O), and 10 μm in (P).

in vitro[24] and *in vivo*.[25] Months after transplantation, differentiated human neurons were still premature, and there were even many undifferentiated NSCs or NPCs.[20] Although at an early stage differentiated neurons were integrated into host neural circuits promoting functional recovery, at a later stage, more neurons, new types of neurons and even astrocytes[25,26] were generated, which could either properly or inappropriately innervate host neurons, causing further functional improvement[25] or maladaptive function,[27] respectively. Third, the potential risk of transplantation of hPSC-derived cells is tumor formation. Indeed, human iPSC-derived NSCs initially promoted functional recovery after SCI at an early stage after transplantation; however, at a later stage, there was oncogenic transformation within the graft accompanied by deteriorated function.[28] Taken together, it is essential to extend the observation period of animals with human NPC transplantation to fully identify the fate and to verify the safety of grafted cells before initiating clinical trials.

Here, we transplanted human ESC-derived spinal dorsal interneuron (dI4/dIL$_A$) NPCs into the adult naive rat spinal cord in an effort to characterize their long-term fate and safety over 1 year. Because the anatomy of the spinal cord and neural function of naive rats were normal, any potential lesion to the spinal cord and harmful event that led to neural dysfunction could be easily detected. In addition, there were also several studies where cells were transplanted into the naive spinal cord to demonstrate safety.[20,26] All grafted NPCs had undergone differentiation, yielding mainly GABA neurons and astrocytes. Fully mature human neurons grew many axons and formed numerous synapses with rat neural circuits, together with mature human astrocytes that structurally integrated into the rat spinal cord. The sensorimotor function of rats was not impaired by intraspinal transplantation, even when human neurons were activated or inhibited by designer receptors exclusively activated by designer drugs (DREADDs).[29]

RESULTS

Human ESC-derived dorsal spinal GABA neurons survived long-term and fully matured in the rat spinal cord

Adult naive athymic nude rats received transplantation of either human ESC-derived dorsal spinal dI4/dIL$_A$ NPCs with or without BiDREADD expression (dI4-Bi-DREADDs, dI4) or culture medium without cells (Medium) into the cervical enlargement (C6-C8) of the spinal cord. Twelve months later, the rats were sacrificed. The general morphology of the brains and spinal cords was comparable between the three groups, with no obvious lesions detected (Figure S1A). By immunostaining with human nuclei (hNu), mCherry and HA (reporters for hM3Dq and KORD, respectively), grafted human cells were identified (Figure 1A) mainly in the gray matter (GM), with many human cells also migrating into the white matter (WM). Within the graft, approximately 60% of human cells had differentiated into NeuN$^+$ neurons (Figure 1B). Along the anterior-posterior (AP) axis of the central nervous system (CNS), human neurons expressed few, if any, adult forebrain markers, including FOXG1 and OTX2, and the hindbrain marker HOXA3 (Figure S1B). Interestingly, human neurons silenced the expression of HOXB4 and HOXC8, transcription factors (TFs) that are highly expressed during spinal cord development (Figure S1B). Along the dorsal-ventral (DV) axis of the spinal cord, approximately 90% of human neurons express the dI4/dIL$_A$-specific marker PTF1A (Figure 1C).[16] Approximately 40% of human neurons were PAX2$^+$ (Figure 1C), a marker of inhibitory neurons in the adult spinal cord. A few neurons from other spinal domains were also detected, including BRN3A, LMX1B, BHLHB5, FOXP2, CHX10, ISLET1 and SIM1 (Figure S1C). In the neurotransmitter phenotype, a large amount of GABA was deposited within the graft (Figure 1E), suggesting that the majority of human neurons were GABAergic, while some human neurons were calcium/calmodulin-dependent kinase IIα (CaMKIIα)$^+$ glutamatergic, a few were choline acetyltransferase (ChAT)$^+$ cholinergic, and no glycine transporter 2 (GlyT2)$^+$ glycinergic, 5-hydroxytryptamine (5-HT)$^+$ serotoninergic or tyrosine hydroxylase (TH)$^+$ dopaminergic (Figure S1D). Of the human GABAergic neurons, several subtypes were identified, including parvalbumin (PV), calbindin (CB) and neuronal nitric oxide synthase (n-NOS), while neuropeptide Y (NPY) and RAR-related orphan receptor β (RORβ) were not detected (Figure S1E). In the injured monkey spinal cord in our previous study,[18] the same subtypes of spinal GABAergic neurons were also detected, including PV, CB and n-NOS but not NPY and RORβ (Figure S1F).

Human neurons extensively expressed neuronal-specific enolase (NSE), human mitochondria (hMito) and potassium-chloride cotransporter-2 (KCC2) (Figures 1F–1H) but not doublecortin (DCX) (Figure S1G), a marker of immature migrating neurons. Human neurons had grown large numbers of human microtube-associated protein-2 (hMAP2)$^+$ dendrites and β-III-tubulin (Tuj1)$^+$ axons within the graft (Figures 1I and 1J); importantly, they were negative for growth-associated protein 43 (GAP43) (Figure S1G), which is highly expressed in growing axons. Specifically, human axons, as verified by human tau (hTau), had extensively grown within the rat spinal cord (Figure 1K). They were densely intermingled within the graft (Figure 1L). Moreover, human axons traveled into the WM (Figure 1M) and projected into the GM, including the

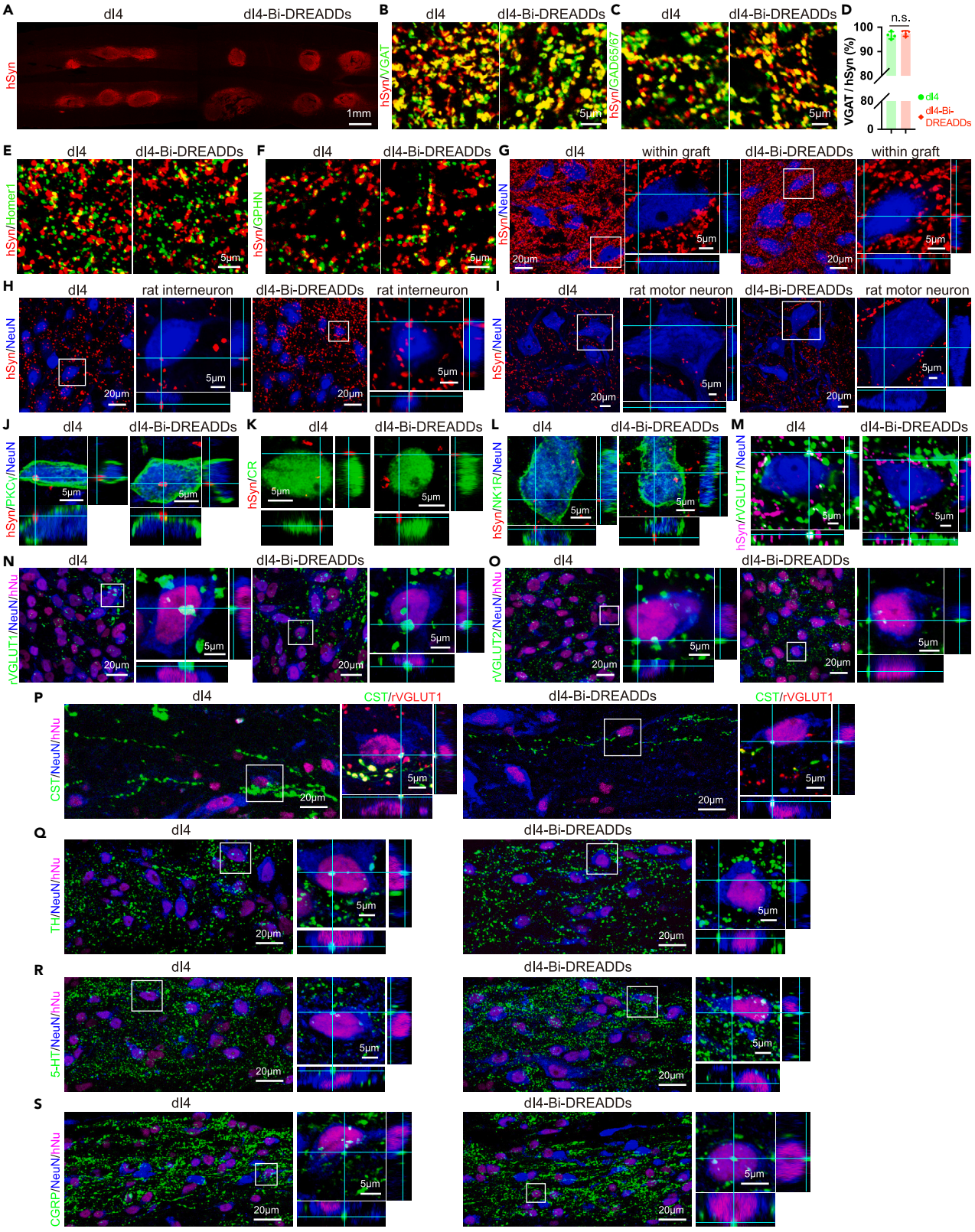
A
dl4
dl4-Bi-DREADDs
hSyn
1mm
B
dl4
dl4-Bi-DREADDs
hSyn/VGAT
5μm
C
dl4
dl4-Bi-DREADDs
hSyn/GAD65/67
5μm
D
n.s.
VGAT / hSyn (%)
100
90
80
80
0
dl4
dl4-Bi-DREADDs
E
dl4
dl4-Bi-DREADDs
hSyn/Homer1
5μm
F
dl4
dl4-Bi-DREADDs
hSyn/GPHN
5μm
G
dl4
within graft
dl4-Bi-DREADDs
within graft
hSyn/NeuN
20μm
5μm
H
dl4
rat interneuron
dl4-Bi-DREADDs
rat interneuron
hSyn/NeuN
I
dl4
rat motor neuron
dl4-Bi-DREADDs
rat motor neuron
hSyn/NeuN
J
dl4
dl4-Bi-DREADDs
hSyn/PKCγ/NeuN
K
dl4
dl4-Bi-DREADDs
hSyn/CR
L
dl4
dl4-Bi-DREADDs
hSyn/NK1R/NeuN
M
dl4
dl4-Bi-DREADDs
hSyn/rVGLUT1/NeuN
N
dl4
dl4-Bi-DREADDs
rVGLUT1/NeuN/hNu
O
dl4
dl4-Bi-DREADDs
rVGLUT2/NeuN/hNu
P
dl4
CST/rVGLUT1
dl4-Bi-DREADDs
CST/rVGLUT1
CST/NeuN/hNu
Q
dl4
dl4-Bi-DREADDs
TH/NeuN/hNu
R
dl4
dl4-Bi-DREADDs
5-HT/NeuN/hNu
S
dl4
dl4-Bi-DREADDs
CGRP/NeuN/hNu

Figure 2. Human dorsal spinal GABA neurons integrated into rat neural circuits

(A) Representative images of horizontal sections of rat C5–C8 spinal cords showing tremendous expression of the presynaptic marker hSyn, indicating the potential formation of human synapses.

(B–F) Images showing that human synapses were established and were mainly inhibitory GABAergic. Many $hSyn^+$ were colocalized with the inhibitory presynaptic markers GAD65/57 (B) and VGAT (C) and were in close apposition with the postsynaptic marker Homer1 (E) and the inhibitory postsynaptic marker GPHN (F). Quantification of the proportion of GAD65/67 (D).

(G) Within the graft, human neurons formed extensive synapses between themselves.

(H–M) Out of the graft but within the GM of rat spinal cords, human neurons formed synapses with rat neurons, including MNs (I), INs (H), such as $PKC\gamma^+$ (J), CR^+ (K), and $NK1R^+$ (L) neurons, and with $rVGLUT1^+$ afferent sensory terminals (M).

(N and O) Images of the graft showing hNu^+NeuN^+ human neurons were innervated by rat excitatory synapses as revealed by rVGULT1 and rVGLUT2.

(P–S) Images of the graft showing hNu^+NeuN^+ human neurons were innervated by rat neural circuits, including the CST from forelimb M1/S1 (P), TH^+ ceruleospinal tract (Q), $5\text{-}HT^+$ raphespinal tract (R), and $CGRP^+$ nonmyelinating peptidergic nociceptive afferents (S). Data are represented as the mean ± SEM. n represents number of rats per group. See also Figure S2. Scale bar, 1 mm in (A), 20 μm in (G–I) and (N–S), and 5 μm in (B–F), (J-M) and in images of magnified white box areas (G–I) and (N–S).

interneuron (IN) and motor neuron (MN) regions (Figures 1N and 1O), while human axons were not wrapped by the rat myelin sheath (Figure 1P). Human axons also projected rostrally into the C1-C4 segments and caudally into the thoracic T3–T5 segments (Figure S2A), mainly in the dorsal horn (DH) rather than in the ventral horn (VH) (Figure S2B), but not into the brain (Figure S2E). Taken together, these results demonstrated the long-term survival, full maturation and extensive axon growth of human spinal GABA neurons in the rat spinal cord.

Human dorsal spinal GABA neurons integrated into rat neural circuits

Human neurons extensively expressed the presynaptic protein human synaptophysin (hSyn) in the rat spinal cord (Figure 2A). Many hSyn coexpressed inhibitory presynaptic markers, including vesicular GABA transporter (VGAT) and glutamate decarboxylase 65/67 kDa (GAD65/67) (Figures 2B–2D). Meanwhile, hSyn was in close apposition with the postsynaptic marker Homer1, especially the inhibitory postsynaptic marker gephyrin (GPHN) (Figures 2E and 2F). Thus, human neurons have established many synapses in the rat spinal cord. These human synapses were densely formed within the graft (Figures 2A and 2G), probably between the human neurons themselves. However, many human synapses were also present outside of the graft, innervating the rat INs and MNs (Figures 2H and 2I). Human neurons also formed synapses with rat protein kinase C gamma (PKCγ) and calretinin (CR) interneurons that potentiate allodynia and neurokinin-1 receptor (NK1R) projection neurons that transmit pain to supraspinal centers (Figures 2J–2L). Importantly, human neurons formed synapses with rat afferent sensory terminals (Figure 2M), as identified by rat-specific vesicular glutamate transporter 1 (rVGLUT1). In addition, many human synapses were also found in the GM of the C1-C4 and T3-T5 segments (Figure S2C), mainly in the DH rather than in the VH (Figure S2D), but not in the brain (Figure S2E).

On the other hand, many rat excitatory synapses, as revealed by rVGLUT1 and rVGLUT2, were present within the graft and innervated human neurons (Figures 2N and 2O). Importantly, corticospinal tract (CST) fibers originating from the bilateral primary sensorimotor cortex (M1/S1) of rat forelimbs were present within the graft, and these CST fibers formed excitatory $rVGLUT1^+$ synapses with human neurons (Figure 2P). Similarly, the rat descending TH^+ ceruleospinal tract (CeST) and $5\text{-}HT^+$ raphespinal tract (RST) were also present within the graft, creating dense innervation with human neurons (Figures 2Q and 2R). In addition, calcitonin gene-related peptide $(CGRP)^+$ nonmyelinating peptidergic nociceptive afferents were also present within the graft and established synapses with human neurons (Figure 2S). Taken together, these results indicated that human neurons could extensively integrate into rat neural circuits.

Differentiation and integration of mature human astrocytes into the rat spinal cord

As the long-term survival of human neurons requires nutrients and oxygen, we investigated the status of blood vessels supplying the graft. Indeed, there were many rat endothelial cell antigen $(RECA\text{-}1)^+$ capillaries within the graft (Figure 3A). The total length, average length, total junctions, and total ending points of capillaries within the graft were comparable to those in the GM, where only rat neurons were present, and were significantly higher than those in the WM (Figures 3A and 3B). Importantly, the coverage and mean fluorescence intensity (MFI) of laminin, a component of the basement membrane, in the graft was comparable to that in both the GM and WM (Figure 3C), suggesting a normal structure of the blood–spinal cord barrier (BSCB) of capillaries within the graft.

Since the normal function of neurons is supported by glia, we investigated whether there was glial differentiation from grafted human cells. Indeed, within the graft, approximately 40% of human cells had differentiated into $SOX9^+$ astrocytes (Figure 3D), with minimal generation of oligodendroglia lineages (Figure 3E). Furthermore, these human astrocytes expressed mature structural and functional proteins, including vimentin, glial fibrillary acidic protein (GFAP), S100β, ALDH1L1 and AQP4 (Figures 3F–3J). By staining with human GFAP (hGFAP), numerous human astrocytes were present not only within the graft but also in the WM, including the lateral and dorsal columns (Figure 3K). Large numbers of $hGFAP^+$ processes of human astrocytes surrounded not only human neurons but also neighboring rat INs and MNs (Figure 3L). Moreover, these processes expressed the gap junction protein connexin 43 (Cx43) (Figure 3M) and glutamate transporter-1 (GLT-1) (Figure 3N), which is responsible for glutamate clearance. The processes of human astrocytes were also aligned with the dendrites and axons of human neurons (Figures 3O and 3P). In addition, the processes of human astrocytes extensively wrapped the rat capillaries (Figure 3Q) and formed $AQP4^+$ endfeet on capillaries (Figure 3R), contributing to the structure of the BSCB. Beyond the C6-C8 segments, many human cells migrated both rostrally into the C1-C4 segments and caudally into the T3-T5 segments (Figure S3A), almost in the WM but not the GM (Figure S3B). Moreover, these migrated human cells were not $NeuN^+$ neurons but $SOX9^+$ astrocytes (Figure S3B). This finding was further

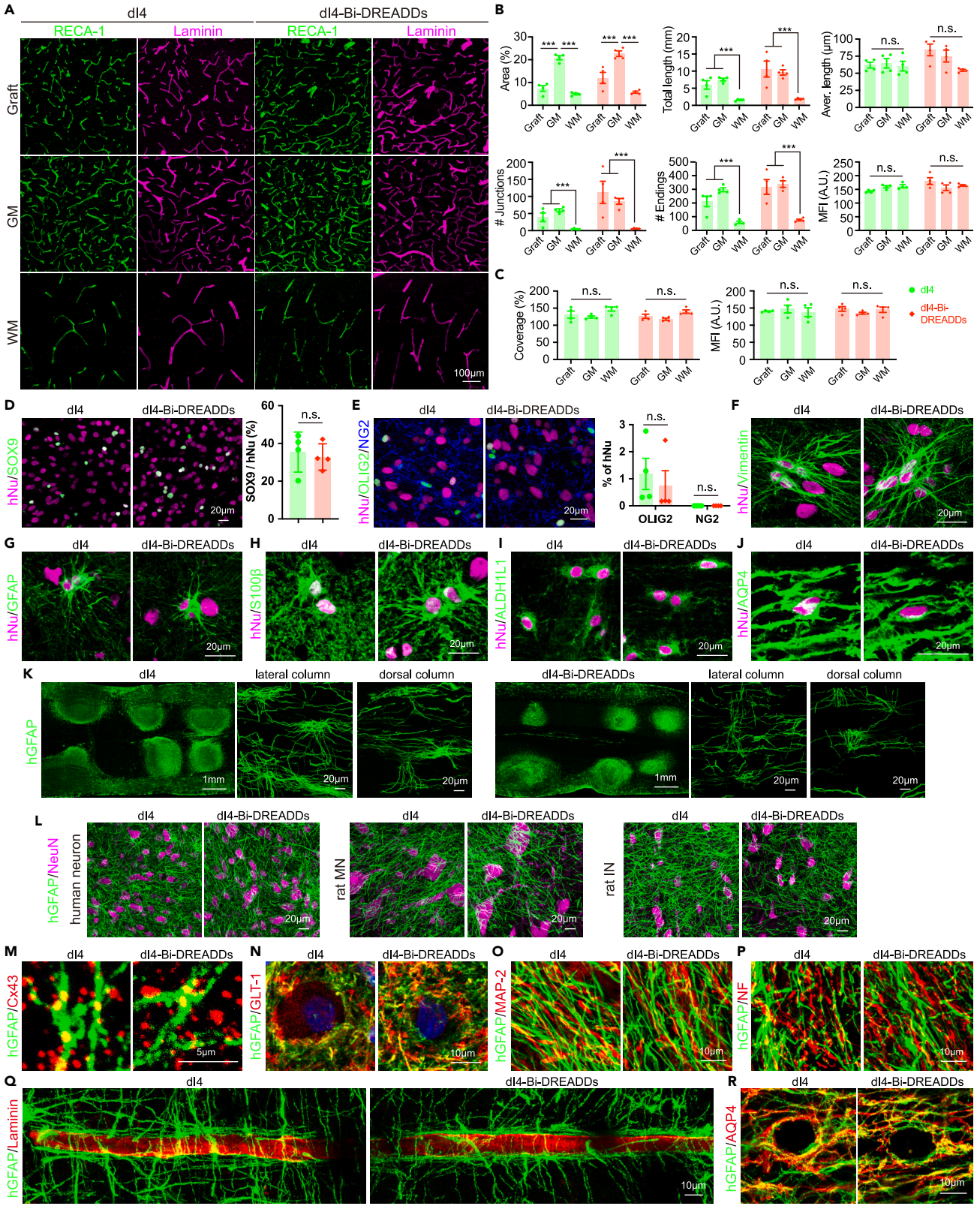
A
dI4
dI4-Bi-DREADDs
RECA-1
Laminin
Graft
GM
WM
100μm
B
Area (%)
Total length (mm)
Aver. length (μm)
Junctions
Endings
MFI (A.U.)
n.s.
***
Graft
GM
WM
C
Coverage (%)
MFI (A.U.)
dI4
dI4-Bi-DREADDs
D
hNu/SOX9
SOX9 / hNu (%)
E
hNu/OLIG2/NG2
% of hNu
OLIG2
NG2
F
hNu/Vimentin
G
hNu/GFAP
H
hNu/S100β
I
hNu/ALDH1L1
J
hNu/AQP4
20μm
K
hGFAP
lateral column
dorsal column
1mm
L
hGFAP/NeuN
human neuron
rat MN
rat IN
M
hGFAP/Cx43
5μm
N
hGFAP/GLT-1
O
hGFAP/MAP-2
P
hGFAP/NF
10μm
Q
hGFAP/Laminin
R
hGFAP/AQP4

Figure 3. Differentiation and integration of mature human astrocytes into the rat spinal cord

(A) Representative images of RECA-1$^+$ capillaries and their associated laminin$^+$ basement membrane in the graft, GM and WM of rat spinal cords.

(B) Quantification of the area, total length, average length, total junctions, total ending points and MFI of RECA-1$^+$ capillaries.

(C) Quantification of coverage of laminin$^+$ basement membrane on RECA-1$^+$ capillaries and MFI of laminin.

(D and E) Images of grafts showing the differentiation of hNu$^+$SOX9$^+$ human astrocytes and hNu$^+$OLIG2$^+$/NG2$^+$ human oligodendroglia lineage cells. Quantification of SOX9 and OLOG2/NG2 revealed that the differentiation of human astrocytes was greater than that of oligodendrocytes.

(F–J) Images of grafts showing differentiated human astrocytes expressing vimentin (F), GFAP (G), S100β (H), ALDH1L1 (I), and AQP4 (J), suggesting their maturation.

(K) Representative images of horizontal sections of rat C5–C8 spinal cords showing tremendous expression of hGFAP in the graft and WM, including the lateral and dorsal columns, indicating extensive differentiation and migration of human astrocytes.

(L) Images showing hGFAP$^+$ processes of human astrocytes densely surrounding human neurons within the graft and rat MNs and INs outside of the graft.

(M and N) Images showing hGFAP$^+$ processes of human astrocytes expressing the gap junction proteins Cx43 (M) and GLT-1, which are responsible for glutamate clearance (N).

(O and P) Images of the graft showing hGFAP$^+$ processes of human astrocytes were aligned with the MAP2$^+$ dendrites and NF$^+$ axons of human neurons.

(Q and R) Images showing hGFAP$^+$ processes of human astrocytes wrapping laminin$^+$ capillaries (Q) and expressing AQP4 contributing to the structure of BSCB (R). Data are represented as the mean ± SEM. n represents number of rats per group. See also Figure S3. Scale bar, 1 mm in (K), 100 μm in (A), 20 μm in (D-L), 10 μm in (N-R), and 5 μm in (M).

verified by hGFAP staining (Figures S3C and S3D). Human cells or human astrocytes did not migrate into the rat brain (Figure S3E). Taken together, these results suggested that extensive human astrocytes were generated and integrated into the rat spinal cord to support the function of human neurons.

Long-term safety of intraspinal transplantation of human ESC-derived dorsal spinal GABA NPCs

In a separate group, human ESCs were directly grafted into the T8 spinal cords of three adult naive nude rats. Deficits in hindlimb locomotion occurred starting from 2 weeks after transplantation, together with the gradual presence of urine retention. By 4 weeks, the rats had full paralysis in the hindlimbs and poor bladder function and were thus euthanized. There were large lesions invading the spinal cords both rostrally and caudally (Figure S4A). The normal morphology of the spinal cord was completely disrupted (Figure S4B), with ectoderm-, mesoderm- and endoderm-like tissues present (Figure S4C). The rat spinal cords were fully occupied by human cells, and there were no human or rat neurons present (Figure S4D), while there were many SOX1$^+$ and human nestin (hNestin)$^+$ NSCs that were highly proliferative (Figure S4E). These results suggested that ESC transplantation can cause teratoma formation and functional loss.

In contrast, in the spinal cords of rats receiving grafts of dI4/dIL$_A$ NPCs, no OCT4$^+$ or NANOG$^+$ human ESCs were detected (Figure S4F). However, a few SOX1$^+$ NSCs and Ki67$^+$ proliferating cells were still preserved (Figure S4F), but these proliferating cells were not hNestin+ NSCs (Figure S4F). In addition, human cells did not undergo apoptosis (Figure S4G). The survival rate and body weight of rats were not influenced by transplantation (Figures S4H and S4I). The weights of integral organs, including spinal cords, brains, hearts, livers, spleens, lungs and kidneys, were comparable between groups (Figures S4J–S4P). Additionally, no lesions or human cells were detected in these organs (Figures S4Q and S4R). Importantly, in sensory function, both mechanical allodynia (Figure 4A) and thermal hyperalgesia (Figure 4B) in the fore and hind paws of rats were comparable among the three groups. Regarding motor function, neither forelimb grooming function (Figure 4C) nor hindlimb overground locomotion (Figure 4D) were impaired by transplantation. Moreover, skilled quadrupedal locomotion involving both forelimbs and hindlimbs was also not impaired (Figure 4E). Finally, by using principal component analysis (PCA) of multiple gait parameters (Table S1), we confirmed that rats with cell transplantation had the same locomotion as control rats (Figure 4F). Since human neurons still maintained the expression of BiDREADDs (Figure 4G) and could indeed be activated by clozapine-N-oxide (CNO) to induce the expression of c-FOS (Figure 4H), we further probed whether the function of rats could be influenced after manipulation of the activity of human neurons. Mechanical allodynia (Figure 4I), thermal hyperalgesia (Figure 4J) and skilled locomotion (Figure 4K) in both fore and hind paws were unaltered after neither activation nor inhibition with CNO and salvinorin B (SalB), respectively. Taken together, these results clearly indicated the long-term safety of intraspinal transplantation of human ESC-derived dorsal spinal GABA NPCs.

DISCUSSION

Here, to the best of our knowledge, this was the first study in which the long-term fate and safety of human ESC-derived dorsal spinal dI4/dIL$_A$ NPCs were demonstrated in adult naive rat spinal cords over 1 year. Before this, there was only one study in which the long-term fate of hPSC-derived forebrain NSCs was identified in injured rat spinal cord over 1.5 years.[25] However, human forebrain neurons mature much more slowly than spinal neurons, and spinal neurons were proven to be better than forebrain neurons for treating SCI.[21,30,31] Thus, our current study laid the foundation for the clinical translation of hPSC-derived spinal NPCs to initiate clinical trials to further verify their safety in SCI patients.

The majority of differentiated human neurons were PTF1A$^+$, and there was little expression of markers of the forebrain, hindbrain and other spinal domains, suggesting that they faithfully preserved spinal dI4/dIL$_A$ identity *in vivo*. Interestingly, the expression of HOXB4 and HOXC8 was silenced in human neurons. Many *Hox* genes are highly expressed in spinal neurons during embryonic human spinal cord development[32–35] and in differentiated spinal neurons from human PSCs.[21] Our human spinal dI4/dIL$_A$ neurons highly expressed HOXB4 and HOXC8 *in vitro*.[17] More than 7 months after transplantation, they still express HOXB4 and HOXC8.[18] However, 12 months after transplantation, the expression of HOXB4 and HOXC8 was almost silenced, which is consistent with the fact that many *Hox* genes are minimally

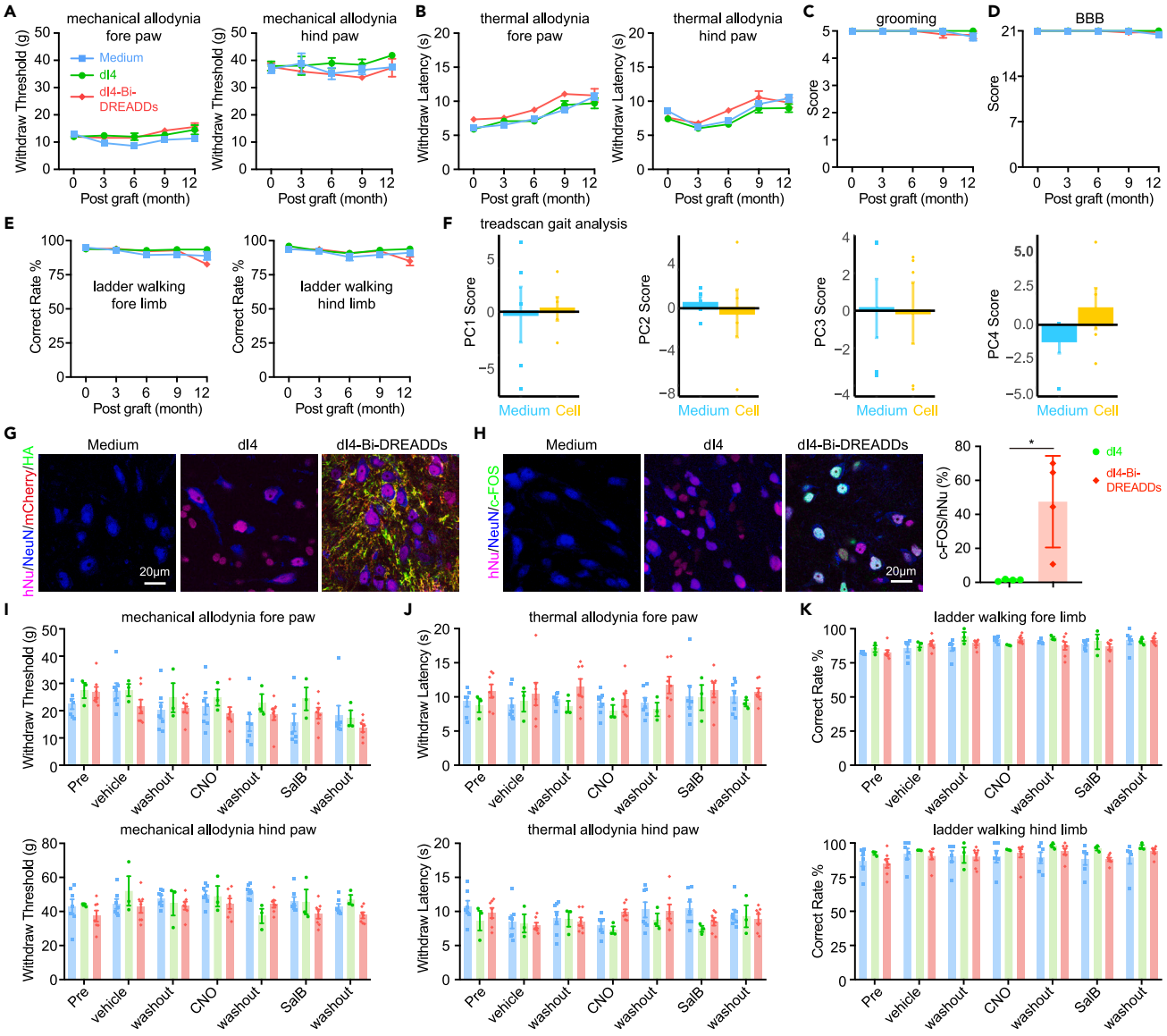

Figure 4. Long-term safety of intraspinal transplantation of human dorsal spinal GABA NPCs

(A and B) Sensory function of rats in the Medium, dI4 and dI4-Bi-DREADDs groups over 12 months post-transplantation. No significant difference was detected in mechanical allodynia (A) and thermal hyperalgesia (B) in the fore and hind paws of rats.

(C–F) Motor function of rats in the Medium, dI4 and dI4-Bi-DREADDs groups over 12 months post-transplantation. Forelimb grooming behavior (C), hindlimb overground locomotion (D), fore- and hindlimb skilled locomotion (E), and gait (F) were unaltered by transplantation.

(G) Images of the grafts showing hNu^+NeuN^+ human neurons in dI4-Bi-DREADDs but not dI4, or hNu^-NeuN^+ rat neurons, still preserved the expression of mCherry and HA, the reporters for hM3Dq and KORD, respectively.

(H) Images of the grafts showing hNu^+NeuN^+ human neurons in dI4-Bi-DREADDs but not dI4 or hNu^-NeuN^+ rat neurons expressing c-FOS upon CNO activation. Quantification of the proportion of c-FOS suggested that human neurons were activated by CNO.

(I and J) Sensory function of rats in the Medium, dI4 and dI4-Bi-DREADDs groups at 12 months post-transplantation under BiDREADDs manipulation. No significant difference was detected in mechanical allodynia (I) and thermal hyperalgesia (J) in the fore and hind paws of rats after CNO, SalB or vehicle application.

(K) Motor function of rats in the Medium, dI4 and dI4-Bi-DREADDs groups at 12 months post-transplantation under BiDREADDs manipulation. No significant difference was detected in skilled locomotion in the fore and hind paws of rats after CNO, SalB or vehicle application. Data are represented as the mean ± SEM. n represents number of rats per group. See also Figure S4 and Table S1. Scale bar, 20 μm in (G and H).

expressed in spinal neurons of adult monkeys[36] and humans.[37] Thus, the silenced expression of *Hox* genes in human neurons could demonstrate their maturity. Indeed, human neurons evenly express high levels of NSE, KCC2, and especially numerous mitochondria, whose amount directly determines the maturity of neurons.[38] In addition, human neurons have numerous mature dendrites and axons and have established

tremendous synapses. Thus, human dorsal spinal neurons could fully mature at least 1 year after transplantation, in contrast to the more protracted time for human forebrain neurons to mature.[25] Human axons were unmyelinated, and the putative reason is that myelination is unnecessary for spinal interneurons that transmit information shortly and locally; another possibility is that the origin of axons and myelin is different in species since axons of grafted rat spinal neurons could be wrapped by host rat myelin.[39]

In the naive adult rodent spinal cord, dI4/dIL$_A$ GABA neurons contribute to both the presynaptic inhibition of afferent sensory terminals[40] and postsynaptic inhibition of sensory interneurons, playing pivotal roles in preventing abnormal sensation,[41,42] regulating muscle tone,[43] and securing the smoothness of forelimb grasping[44] and hindlimb locomotion.[45] Our grafted human dorsal spinal GABA neurons projected axons mainly to the DH rather than the VH and similarly formed inhibitory synapses mainly with DH interneurons rather than VH motor neurons. Importantly, they formed synapses with rat PKCγ,[46] CR interneurons[47,48] and NK1R nociception projection neurons[49] and established presynaptic inhibition structures with rat afferent sensory terminals, which is consistent with the projections of rodent spinal dI4/dIL$_A$ neurons. Meanwhile, human dorsal spinal GABA neurons were innervated by rat neural circuits, including CST, CeST, RST and CGRP sensory afferents, consistent with the results obtained by retrograde monosynaptic rabies virus tracing of rodent spinal dI4/dIL$_A$ neurons.[41] Thus, regionally specified neurons, when grafted *in vivo*, could specifically find their appropriate targets and be innervated properly by specific host circuits, which implies that for precisely reconstructing damaged circuits after SCI, subtypes of molecularly defined neurons might be optimal over a mixture of unspecified populations.

The normal function of neurons is critically supported by glial cells. In addition to neurons, human dorsal spinal dI4/dIL$_A$ NPCs also almost exclusively produced tremendous mature astrocytes that not only colonized within the graft but also extensively migrated in the WM, consistent with our previous[26] and other studies.[25,50] Few oligodendroglia lineages were yielded, which could be explained by the fact that in the developing human spinal cord, astrocytes and oligodendroglia are generated from the dorsal and ventral parts, respectively.[35] The expression of many structural and functional proteins in human astrocytes enables them to execute functions, including supporting the growth of dendrites and axons, clearance of glutamate and constitution of the BSCB. Indeed, the structure of the BSCB within the graft was normal, which could prevent harmful agents from infiltrating into the parenchyma to cause neuronal death. Importantly, human neurons could be activated by DREADDs and did not undergo apoptosis, suggesting that they were authentically alive. By virtue of human astrocytes and normal BSCB, human neurons could be anticipated to continue to survive permanently.

Although mature human neurons and astrocytes survived long-term and integrated into the rat spinal cord, the sensorimotor function of rats was not impaired by cell transplantation. This clearly demonstrated the long-term safety of intraspinal transplantation of cells, while on the other hand, it implied that synapses formed between human and rat neurons may be nonfunctional, which is further strengthened by the fact that sensorimotor function of rats was still unchanged after BiDREADD modulation of human neuron activity. It might be impossible that the human synapses observed by immunofluorescence were not authentic synapses because the postsynaptic markers were present and in close apposition with presynaptic markers; in addition, immunofluorescence of synaptic markers in the adult CNS can directly represent synapses. Because the neural circuits of adult naive rats have already been normally and well developed, which means that no neural plasticity is needed, there is no need for grafted human neurons to execute their function. If human neurons are grafted into the spinal cords of newborn rats, they could develop together with rat neurons and functionally integrate into host circuits, as was observed in human brain organoid transplantation.[51] Importantly, when the CNS is injured, adult neurons regress to an embryonic growth state[52,] and neural plasticity occurs.[53] Neurons grafted into this injured environment can then functionally integrate into host circuits and exert neural function.

In summary, the long-term safety of human ESC-derived dorsal spinal dI4/dIL$_A$ NPCs in the spinal cord was verified in naive adult rats. To enter into clinical trials, they must merit the cell quality control as proposed in the guidelines,[54] such as detecting composition and relevant cytokines, genetic or other manipulations. Future work will address these concerns.

Limitations of the study

Although the long-term fate and safety of intraspinal human ESC-derived dorsal spinal dI4/dIL$_A$ NPCs was verified in naive adult rats, further long-term studies in SCI rats and even in NHPs are clearly needed to definitively validate their fate, efficacy, and safety before initiating any clinical trials. In addition, immunoelectron microscopy, virus tracing and electrophysiology studies, although relatively technically hard, are needed to faithfully prove that grafted human neurons are functionally integrated into host neural circuits. This work is now underway in our successive research.

STAR★METHODS

Detailed methods are provided in the online version of this paper and include the following:

- KEY RESOURCES TABLE
- RESOURCE AVAILABILITY
  - Lead contact
  - Materials availability
  - Data and code availability
- EXPERIMENTAL MODEL AND STUDY PARTICIPANT DETAILS
  - Cells
  - Animals

- METHOD DETAILS
  - Cell differentiation
  - Cell transplantation
  - Mechanical allodynia
  - Thermal hyperalgesia
  - Grooming test
  - Open field locomotion
  - Horizontal ladder walking
  - Gait analysis
  - Chemogenetics
  - Corticospinal tract tracing
  - Tissue processing
  - Hematoxylin & eosin staining
  - Immunofluorescence
  - Laser scanning confocal microscopy
- QUANTIFICATION AND STATISTICAL ANALYSIS

SUPPLEMENTAL INFORMATION

Supplemental information can be found online at https://doi.org/10.1016/j.isci.2023.108306.

ACKNOWLEDGMENTS

This work was supported by the Ministry of Science and Technology China (2017ZX09304022, 2022ZD0204704), the Hubei Natural Science Foundation (2020SCZ035), the National Natural Science Foundation of China (82301572) and the China Postdoctoral Science Foundation (2023M731202). The authors acknowledge Fangliang Guo and Jun Huang for animal care during the COVID-19 outbreak.

AUTHOR CONTRIBUTIONS

W.W., H.C., and S-C.Z. conceptualized the study. X.Z., W.W., H.C., and S-C.Z. designed the experiments. J.X, Y.W., and C.G. performed cell differentiation. X.Z. performed cell transplantation, behavioral tests, histology, and immunofluorescence and recorded and analyzed the data. Z.L. performed some immunofluorescence. Z.H. performed gait analysis. R.Z. analyzed part of the data. X.Z. drafted and revised the paper. All of the authors read, edited, and approved the final version of the manuscript.

DECLARATION OF INTERESTS

The authors declare no competing interests.

Received: August 10, 2023
Revised: September 28, 2023
Accepted: October 20, 2023
Published: October 23, 2023

REFERENCES

1. Courtine, G., and Sofroniew, M.V. (2019). Spinal cord repair: advances in biology and technology. Nat. Med. *25*, 898–908. https://doi.org/10.1038/s41591-019-0475-6.
2. Fischer, I., Dulin, J.N., and Lane, M.A. (2020). Transplanting neural progenitor cells to restore connectivity after spinal cord injury. Nat. Rev. Neurosci. *21*, 366–383. https://doi.org/10.1038/s41583-020-0314-2.
3. Zipser, C.M., Cragg, J.J., Guest, J.D., Fehlings, M.G., Jutzeler, C.R., Anderson, A.J., and Curt, A. (2022). Cell-based and stem-cell-based treatments for spinal cord injury: evidence from clinical trials. Lancet Neurol. *21*, 659–670. https://doi.org/10.1016/S1474-4422(21)00464-6.
4. Ribeiro, B.F., da Cruz, B.C., de Sousa, B.M., Correia, P.D., David, N., Rocha, C., Almeida, R.D., Ribeiro da Cunha, M., Marques Baptista, A.A., and Vieira, S.I. (2023). Cell therapies for spinal cord injury: a review of the clinical trials and cell-type therapeutic potential. Brain *146*, 2672–2693. https://doi.org/10.1093/brain/awad047.
5. Huang, H., Chen, L., Moviglia, G., Sharma, A., Al Zoubi, Z.M., He, X., and Chen, D. (2022). Advances and prospects of cell therapy for spinal cord injury patients. J. Neurorestoratol. *10*, 13–30. https://doi.org/10.26599/Jnr.2022.9040007.
6. Sugai, K., Sumida, M., Shofuda, T., Yamaguchi, R., Tamura, T., Kohzuki, T., Abe, T., Shibata, R., Kamata, Y., Ito, S., et al. (2021). First-in-human clinical trial of transplantation of iPSC-derived NS/PCs in subacute complete spinal cord injury: Study protocol. Regen. Ther. *18*, 321–333. https://doi.org/10.1016/j.reth.2021.08.005.
7. Siddall, P.J., McClelland, J.M., Rutkowski, S.B., and Cousins, M.J. (2003). A longitudinal study of the prevalence and characteristics of pain in the first 5 years following spinal cord injury. Pain *103*, 249–257. https://doi.org/10.1016/S0304-3959(02)00452-9.
8. Holtz, K.A., Lipson, R., Noonan, V.K., Kwon, B.K., and Mills, P.B. (2017). Prevalence and Effect of Problematic Spasticity After Traumatic Spinal Cord Injury. Arch. Phys. Med. Rehabil. *98*, 1132–1138. https://doi.org/10.1016/j.apmr.2016.09.124.
9. Nair, K.P.S., and Marsden, J. (2014). The management of spasticity in adults. BMJ Br. Med. *349*, g4737. https://doi.org/10.1136/bmj.g4737.
10. Drew, G.M., Siddall, P.J., and Duggan, A.W. (2004). Mechanical allodynia following contusion injury of the rat spinal cord is associated with loss of GABAergic inhibition in the dorsal horn. Pain *109*, 379–388. https://doi.org/10.1016/j.pain.2004.02.007.
11. Meisner, J.G., Marsh, A.D., and Marsh, D.R. (2010). Loss of GABAergic Interneurons in Laminae I-III of the Spinal Cord Dorsal Horn

Contributes to Reduced GABAergic Tone and Neuropathic Pain after Spinal Cord Injury. J. Neurotrauma *27*, 729–737. https://doi.org/10.1089/neu.2009.1166.

12. Gwak, Y.S., and Hulsebosch, C.E. (2011). GABA and central neuropathic pain following spinal cord injury. Neuropharmacology *60*, 799–808. https://doi.org/10.1016/j.neuropharm.2010.12.030.
13. Alaynick, W.A., Jessell, T.M., and Pfaff, S.L. (2011). Snapshot: Spinal Cord Development. Cell *146*, 178–178.e1. https://doi.org/10.1016/j.cell.2011.06.038.
14. Koch, S.C., Acton, D., and Goulding, M. (2018). Spinal Circuits for Touch, Pain, and Itch. Annu. Rev. Physiol. *80*, 189–217. https://doi.org/10.1146/annurev-physiol-022516-034303.
15. Sengupta, M., and Bagnall, M.W. (2023). Spinal Interneurons: Diversity and Connectivity in Motor Control. Annu. Rev. Neurosci. *46*, 79–99. https://doi.org/10.1146/annurev-neuro-083122-025325.
16. Glasgow, S.M., Henke, R.M., MacDonald, R.J., Wright, C.V.E., and Johnson, J.E. (2005). Ptf1a determines GABAergic over glutamatergic neuronal cell fate in the spinal cord dorsal horn. Development *132*, 5461–5469. https://doi.org/10.1242/dev.02167.
17. Gong, C., Zheng, X., Guo, F., Wang, Y., Zhang, S., Chen, J., Sun, X., Shah, S.Z.A., Zheng, Y., Li, X., et al. (2021). Human spinal GABA neurons alleviate spasticity and improve locomotion in rats with spinal cord injury. Cell Rep. *34*, 108889. https://doi.org/10.1016/j.celrep.2021.108889.
18. Zheng, X., Zhu, B., Xu, J., Liu, D., Huang, Y., Chen, D., Liu, Z., Guo, F., Dong, Y., Zhu, W., et al. (2023). Human spinal GABA neurons survive and mature in the injured nonhuman primate spinal cord. Stem Cell Rep. *18*, 439–448. https://doi.org/10.1016/j.stemcr.2022.12.016.
19. Lu, P., Woodruff, G., Wang, Y., Graham, L., Hunt, M., Wu, D., Boehle, E., Ahmad, R., Poplawski, G., Brock, J., et al. (2014). Long-Distance Axonal Growth from Human Induced Pluripotent Stem Cells after Spinal Cord Injury. Neuron *83*, 789–796. https://doi.org/10.1016/j.neuron.2014.07.014.
20. Fandel, T.M., Trivedi, A., Nicholas, C.R., Zhang, H., Chen, J., Martinez, A.F., Noble-Haeusslein, L.J., and Kriegstein, A.R. (2016). Transplanted Human Stem Cell-Derived Interneuron Precursors Mitigate Mouse Bladder Dysfunction and Central Neuropathic Pain after Spinal Cord Injury. Cell Stem Cell *19*, 544–557. https://doi.org/10.1016/j.stem.2016.08.020.
21. Kumamaru, H., Kadoya, K., Adler, A.F., Takashima, Y., Graham, L., Coppola, G., and Tuszynski, M.H. (2018). Generation and post-injury integration of human spinal cord neural stem cells. Nat. Methods *15*, 723–731. https://doi.org/10.1038/s41592-018-0074-3.
22. Khazaei, M., Ahuja, C.S., Nakashima, H., Nagoshi, N., Li, L., Wang, J., Chio, J., Badner, A., Seligman, D., Ichise, A., et al. (2020). GDNF rescues the fate of neural progenitor grafts by attenuating Notch signals in the injured spinal cord in rodents. Sci. Transl. Med. *12*, eaau3538. https://doi.org/10.1126/scitranslmed.aau3538.
23. Savic, G., DeVivo, M.J., Frankel, H.L., Jamous, M.A., Soni, B.M., and Charlifue, S. (2017). Long-term survival after traumatic spinal cord injury: a 70-year British study. Spinal Cord *55*, 651–658. https://doi.org/10.1038/sc.2017.23.
24. Nicholas, C.R., Chen, J., Tang, Y., Southwell, D.G., Chalmers, N., Vogt, D., Arnold, C.M., Chen, Y.J.J., Stanley, E.G., Elefanty, A.G., et al. (2013). Functional Maturation of hPSC-Derived Forebrain Interneurons Requires an Extended Timeline and Mimics Human Neural Development. Cell Stem Cell *12*, 573–586. https://doi.org/10.1016/j.stem.2013.04.005.
25. Lu, P., Ceto, S., Wang, Y., Graham, L., Wu, D., Kumamaru, H., Staufenberg, E., and Tuszynski, M.H. (2017). Prolonged human neural stem cell maturation supports recovery in injured rodent CNS. J. Clin. Invest. *127*, 3287–3299. https://doi.org/10.1172/Jci92955.
26. Chen, H., Qian, K., Chen, W., Hu, B., Blackbourn, L.W., Du, Z., Ma, L., Liu, H., Knobel, K.M., Ayala, M., and Zhang, S.C. (2015). Human-derived neural progenitors functionally replace astrocytes in adult mice. J. Clin. Invest. *125*, 1033–1042. https://doi.org/10.1172/Jci69097.
27. Hofstetter, C.P., Holmström, N.A.V., Lilja, J.A., Schweinhardt, P., Hao, J., Spenger, C., Wiesenfeld-Hallin, Z., Kurpad, S.N., Frisén, J., and Olson, L. (2005). Allodynia limits the usefulness of intraspinal neural stem cell grafts; directed differentiation improves outcome. Nat. Neurosci. *8*, 346–353. https://doi.org/10.1038/nn1405.
28. Nori, S., Okada, Y., Nishimura, S., Sasaki, T., Itakura, G., Kobayashi, Y., Renault-Mihara, F., Shimizu, A., Koya, I., Yoshida, R., et al. (2015). Long-Term Safety Issues of iPSC-Based Cell Therapy in a Spinal Cord Injury Model: Oncogenic Transformation with Epithelial-Mesenchymal Transition. Stem Cell Rep. *4*, 360–373. https://doi.org/10.1016/j.stemcr.2015.01.006.
29. Roth, B.L. (2016). DREADDs for Neuroscientists. Neuron *89*, 683–694. https://doi.org/10.1016/j.neuron.2016.01.040.
30. Kadoya, K., Lu, P., Nguyen, K., Lee-Kubli, C., Kumamaru, H., Yao, L., Knackert, J., Poplawski, G., Dulin, J.N., Strobl, H., et al. (2016). Spinal cord reconstitution with homologous neural grafts enables robust corticospinal regeneration. Nat. Med. *22*, 479–487. https://doi.org/10.1038/nm.4066.
31. Dell'Anno, M.T., Wang, X., Onorati, M., Li, M., Talpo, F., Sekine, Y., Ma, S., Liu, F., Cafferty, W.B.J., Sestan, N., and Strittmatter, S.M. (2018). Human neuroepithelial stem cell regional specificity enables spinal cord repair through a relay circuit. Nat. Commun. *9*, 3419. https://doi.org/10.1038/s41467-018-05844-8.
32. Rayon, T., Maizels, R.J., Barrington, C., and Briscoe, J. (2021). Single-cell transcriptome profiling of the human developing spinal cord reveals a conserved genetic programme with human-specific features. Development *148*, dev199711. https://doi.org/10.1242/dev.199711.
33. Zhang, Q., Wu, X., Fan, Y., Jiang, P., Zhao, Y., Yang, Y., Han, S., Xu, B., Chen, B., Han, J., et al. (2021). Single-cell analysis reveals dynamic changes of neural cells in developing human spinal cord. EMBO Rep. *22*, e52728. https://doi.org/10.15252/embr.202152728.
34. Andersen, J., Thom, N., Shadrach, J.L., Chen, X., Onesto, M.M., Amin, N.D., Yoon, S.J., Li, L., Greenleaf, W.J., Müller, F., et al. (2023). Single-cell transcriptomic landscape of the developing human spinal cord. Nat. Neurosci. *26*, 902–914. https://doi.org/10.1038/s41593-023-01311-w.
35. Li, X., Andrusivova, Z., Czarnewski, P., Langseth, C.M., Andersson, A., Liu, Y., Gyllborg, D., Braun, E., Larsson, L., Hu, L., et al. (2023). Profiling spatiotemporal gene expression of the developing human spinal cord and implications for ependymoma origin. Nat. Neurosci. *26*, 891–901. https://doi.org/10.1038/s41593-023-01312-9.
36. Fan, Y., Wu, X., Han, S., Zhang, Q., Sun, Z., Chen, B., Xue, X., Zhang, H., Chen, Z., Yin, M., et al. (2023). Single-cell analysis reveals region-heterogeneous responses in rhesus monkey spinal cord with complete injury. Nat. Commun. *14*, 4796. https://doi.org/10.1038/s41467-023-40513-5.
37. Yadav, A., Matson, K.J.E., Li, L., Hua, I., Petrescu, J., Kang, K., Alkaslasi, M.R., Lee, D.I., Hasan, S., Galuta, A., et al. (2023). A cellular taxonomy of the adult human spinal cord. Neuron *111*, 328–344.e7. https://doi.org/10.1016/j.neuron.2023.01.007.
38. Iwata, R., Casimir, P., Erkol, E., Boubakar, L., Planque, M., Gallego López, I.M., Ditkowska, M., Gasparіunaite, V., Beckers, S., Remans, D., et al. (2023). Mitochondria metabolism sets the species-specific tempo of neuronal development. Science *379*, eabn4705. https://doi.org/10.1126/science.abn4705.
39. Hunt, M., Lu, P., and Tuszynski, M.H. (2017). Myelination of axons emerging from neural progenitor grafts after spinal cord injury. Exp. Neurol. *296*, 69–73. https://doi.org/10.1016/j.expneurol.2017.07.005.
40. Betley, J.N., Wright, C.V.E., Kawaguchi, Y., Erdélyi, F., Szabó, G., Jessell, T.M., and Kaltschmidt, J.A. (2009). Stringent Specificity in the Construction of a GABAergic Presynaptic Inhibitory Circuit. Cell *139*, 161–174. https://doi.org/10.1016/j.cell.2009.08.027.
41. Escalante, A., and Klein, R. (2020). Spinal Inhibitory Ptf1a-Derived Neurons Prevent Self-Generated Itch. Cell Rep. *33*. https://doi.org/10.1016/j.celrep.2020.108422.
42. Mona, B., Villarreal, J., Savage, T.K., Kollipara, R.K., Boisvert, B.E., and Johnson, J.E. (2020). Positive autofeedback regulation of Ptf1a transcription generates the levels of PTF1A required to generate itch circuit neurons. Gene Dev. *34*, 621–636. https://doi.org/10.1101/gad.332577.119.
43. Zhang, J., Weinrich, J.A.P., Russ, J.B., Comer, J.D., Bommareddy, P.K., DiCasoli, R.J., Wright, C.V.E., Li, Y., van Roessel, P.J., and Kaltschmidt, J.A. (2017). A Role for Dystonia-Associated Genes in Spinal GABAergic Interneuron Circuitry. Cell Rep. *21*, 666–678. https://doi.org/10.1016/j.celrep.2017.09.079.
44. Fink, A.J.P., Croce, K.R., Huang, Z.J., Abbott, L.F., Jessell, T.M., and Azim, E. (2014). Presynaptic inhibition of spinal sensory feedback ensures smooth movement. Nature *509*, 43–48. https://doi.org/10.1038/nature13276.
45. Koch, S.C., Del Barrio, M.G., Dalet, A., Gatto, G., Günther, T., Zhang, J., Seidler, B., Saur, D., Schüle, R., and Goulding, M. (2017). ROR beta Spinal Interneurons Gate Sensory Transmission during Locomotion to Secure a Fluid Walking Gait. Neuron *96*, 1419–1431.e5. https://doi.org/10.1016/j.neuron.2017.11.011.
46. Malmberg, A.B., Chen, C., Tonegawa, S., and Basbaum, A.I. (1997). Preserved acute pain and reduced neuropathic pain in mice lacking PKC gamma. Science *278*, 279–283. https://doi.org/10.1126/science.278.5336.279.
47. Petitjean, H., Bourojeni, F.B., Tsao, D., Davidova, A., Sotocinal, S.G., Mogil, J.S.,

Kania, A., and Sharif-Naeini, R. (2019). Recruitment of Spinoparabrachial Neurons by Dorsal Horn Calretinin Neurons. Cell Rep. *28*, 1429–1438.e4. https://doi.org/10.1016/j.celrep.2019.07.048.

48. Smith, K.M., Browne, T.J., Davis, O.C., Coyle, A., Boyle, K.A., Watanabe, M., Dickinson, S.A., Iredale, J.A., Gradwell, M.A., Jobling, P., et al. (2019). Calretinin positive neurons form an excitatory amplifier network in the spinal cord dorsal horn. Elife *8*, e49190. https://doi.org/10.7554/eLife.49190.
49. Mantyh, P.W., Rogers, S.D., Honore, P., Allen, B.J., Ghilardi, J.R., Li, J., Daughters, R.S., Lappi, D.A., Wiley, R.G., and Simone, D.A. (1997). Inhibition of hyperalgesia by ablation of lamina I spinal neurons expressing the substance P receptor. Science *278*, 275–279. https://doi.org/10.1126/science.278.5336.275.
50. Lien, B.V., Tuszynski, M.H., and Lu, P. (2019). Astrocytes migrate from human neural stem cell grafts and functionally integrate into the injured rat spinal cord. Exp. Neurol. *314*, 46–57. https://doi.org/10.1016/j.expneurol.2019.01.006.
51. Revah, O., Gore, F., Kelley, K.W., Andersen, J., Sakai, N., Chen, X., Li, M.Y., Birey, F., Yang, X., Saw, N.L., et al. (2022). Maturation and circuit integration of transplanted human cortical organoids. Nature *610*, 319–326. https://doi.org/10.1038/s41586-022-05277-w.
52. Poplawski, G.H.D., Kawaguchi, R., Van Niekerk, E., Lu, P., Mehta, N., Canete, P., Lie, R., Dragatsis, I., Meves, J.M., Zheng, B., et al. (2020). Injured adult neurons regress to an embryonic transcriptional growth state. Nature *581*, 77–82. https://doi.org/10.1038/s41586-020-2200-5.
53. Anderson, M.A., Squair, J.W., Gautier, M., Hutson, T.H., Kathe, C., Barraud, Q., Bloch, J., and Courtine, G. (2022). Natural and targeted circuit reorganization after spinal cord injury. Nat. Neurosci. *25*, 1584–1596. https://doi.org/10.1038/s41593-022-01196-1.
54. Huang, H.Y., Al Zoubi, Z.M., Moviglia, G., Sharma, H.S., Sarnowska, A., Sanberg, P.R., Chen, L., Xue, Q., Siniscalco, D., Feng, S.Q., et al. (2022). Clinical cell therapy guidelines for neurorestoration (IANR/CANR 2022). J. Neurorestoratol. *10*, 100015. https://doi.org/10.1016/j.jnrt.2022.100015.
55. Xiong, M., Tao, Y., Gao, Q., Feng, B., Yan, W., Zhou, Y., Kotsonis, T.A., Yuan, T., You, Z., Wu, Z., et al. (2021). Human Stem Cell-Derived Neurons Repair Circuits and Restore Neural Function. Cell Stem Cell *28*, 112–126.e6. https://doi.org/10.1016/j.stem.2020.08.014.
56. Xu, J., Huang, L.J., Fang, Z., Luo, H.M., Chen, Y.Q., Li, Y.J., Gong, C.Z., and Chen, H. (2022). Spinal dI4 Interneuron Differentiation From Human Pluripotent Stem Cells. Front. Mol. Neurosci. *15*, 845875. https://doi.org/10.3389/fnmol.2022.845875.
57. Lepore, A.C. (2011). Intraspinal Cell Transplantation for Targeting Cervical Ventral Horn in Amyotrophic Lateral Sclerosis and Traumatic Spinal Cord Injury. J. Vis. Exp. 3069. https://doi.org/10.3791/3069.
58. Martinov, T., Mack, M., Sykes, A., and Chatterjea, D. (2013). Measuring Changes in Tactile Sensitivity in the Hind Paw of Mice Using an Electronic von Frey Apparatus. J. Vis. Exp. e51212. https://doi.org/10.3791/51212.
59. Hargreaves, K., Dubner, R., Brown, F., Flores, C., and Joris, J. (1988). A new and sensitive method for measuring thermal nociception in cutaneous hyperalgesia. Pain *32*, 77–88. https://doi.org/10.1016/0304-3959(88)90026-7.
60. Bertelli, J.A., and Mira, J.C. (1993). Behavioral evaluating methods in the objective clinical assessment of motor function after experimental brachial plexus reconstruction in the rat. J. Neurosci. Methods *46*, 203–208. https://doi.org/10.1016/0165-0270(93)90068-3.
61. Basso, D.M., Beattie, M.S., and Bresnahan, J.C. (1995). A sensitive and reliable locomotor rating scale for open field testing in rats. J. Neurotrauma *12*, 1–21. https://doi.org/10.1089/neu.1995.12.1.
62. Metz, G.A., and Whishaw, I.Q. (2002). Cortical and subcortical lesions impair skilled walking in the ladder rung walking test: a new task to evaluate fore- and hindlimb stepping, placing, and co-ordination. J. Neurosci. Methods *115*, 169–179. https://doi.org/10.1016/S0165-0270(02)00012-2.
63. Beare, J.E., Morehouse, J.R., DeVries, W.H., Enzmann, G.U., Burke, D.A., Magnuson, D.S.K., and Whittemore, S.R. (2009). Gait Analysis in Normal and Spinal Contused Mice Using the TreadScan System. J. Neurotrauma *26*, 2045–2056. https://doi.org/10.1089/neu.2009.0914.
64. Torres-Espin, A., Chou, A., Huie, J.R., Kyritsis, N., Upadhyayula, P.S., and Ferguson, A.R. (2021). Reproducible analysis of disease space via principal components using the novel R package syndRomics. Elife *10*, e61812. https://doi.org/10.7554/eLife.61812.
65. Vardy, E., Robinson, J.E., Li, C., Olsen, R.H.J., DiBerto, J.F., Giguere, P.M., Sassano, F.M., Huang, X.P., Zhu, H., Urban, D.J., et al. (2015). A New DREADD Facilitates the Multiplexed Chemogenetic Interrogation of Behavior. Neuron *86*, 936–946. https://doi.org/10.1016/j.neuron.2015.03.065.
66. Schindelin, J., Arganda-Carreras, I., Frise, E., Kaynig, V., Longair, M., Pietzsch, T., Preibisch, S., Rueden, C., Saalfeld, S., Schmid, B., et al. (2012). Fiji: an open-source platform for biological-image analysis. Nat. Methods *9*, 676–682. https://doi.org/10.1038/Nmeth.2019.
67. Zudaire, E., Gambardella, L., Kurcz, C., and Vermeren, S. (2011). A Computational Tool for Quantitative Analysis of Vascular Networks. PLoS One *6*, e27385. https://doi.org/10.1371/journal.pone.0027385.

STAR★METHODS

KEY RESOURCES TABLE

REAGENT or RESOURCE	SOURCE	IDENTIFIER
Antibodies		
Chicken polyclonal anti-NeuN	Millipore	Cat#ABN91; RRID:AB_11205760
Goat polyclonal anti-mCherry	biorbyt	Cat#orb11618; RRID:AB_2687829
Goat polyclonal anti-5-HT	ImmunoStar	Cat#20079; RRID:AB_572262
Goat polyclonal anti-ChAT	Millipore	Cat#AB144P; RRID:AB_2079751
Goat polyclonal anti-OTX2	R&D Systems	Cat#AF1979; RRID:AB_2157172
Goat polyclonal anti-SOX1	R&D Systems	Cat#AF3369; RRID:AB_2239879
Goat polyclonal anti-SOX9	R&D Systems	Cat#AF1997; RRID:AB_355097
Goat polyclonal anti-OLIG2	R&D Systems	Cat#AF2418; RRID: AB_2157554
Goat polyclonal anti-NANOG	R&D Systems	Cat#AF1997; RRID:AB_355097
Guinea pig polyclonal anti-NeuN	Millipore	Cat#ABN90; RRID:AB_11205592
Guinea pig polyclonal anti-c-FOS	Synaptic System	Cat#226003; RRID:AB_2231974
Guinea pig polyclonal anti-VGAT	Synaptic Systems	Cat#131004; RRID:AB_887873
Guinea pig polyclonal anti-Gephyrin	Synaptic Systems	Cat#147318; RRID:AB_2661777
Guinea pig polyclonal anti-VGLUT1	Millipore	Cat#AB5905; RRID: AB_2301751
Guinea pig polyclonal anti-GlyT2	Synaptic Systems	Cat#272 004; RRID: AB_2619998
Guinea pig polyclonal anti-DCX	Synaptic Systems	Cat#326 004; RRID: AB_2620068
Guinea pig polyclonal anti-GLT-1	Millipore	Cat#AB1783; RRID: AB_90949
Mouse monoclonal anti-human Nuclei	Millipore	Cat#MAB1281; RRID: AB_94090
Mouse monoclonal anti-human GFAP	Takara	Cat#Y40420; RRID: AB_2833249
Mouse monoclonal anti-human Tau	BioLegend	Cat#835201; RRID:AB_2565341
Mouse monoclonal anti-human mitochondria	Millipore	Cat#MAB1273; RRID:AB_94052
Mouse monoclonal anti-human Synaptophysin	Invitrogen	Cat#14-6525-80; RRID:AB_10670424
Mouse monoclonal anti-STEM121	Takara	Cat#Y40410; RRID: AB_2632385
Mouse monoclonal anti-human Nestin	R&D Systems	Cat#MAB1259; RRID:AB_2251304
Mouse monoclonal anti-HOXC8	BioLegend	Cat#920501; RRID: AB_2565339
Mouse monoclonal anti-PTF1A	Santa Cruz Biotechnology	Cat#sc-81972; RRID: AB_2174472
Mouse monoclonal anti-BRN3A	Millipore	Cat#MAB1585; RRID: AB_94166
Mouse monoclonal anti-RECA1	Bio-Rad	Cat#MCA970R; RRID:AB_323297
Rabbit polyclonal anti-mCherry	Abcam	Cat#ab167453; RRID:AB_2571870
Rabbit monoclonal anti-HA	Cell Signaling Technology	Cat#3724; RRID:AB_1549585
Rabbit polyclonal anti-NeuN	Millipore	Cat#ABN78; RRID:AB_10807945
Rabbit polyclonal anti-FOXG1	Abcam	Cat#ab18259; RRID: AB_732415
Rabbit polyclonal anti-HOXA3	Sigma-Aldrich	Cat#HPA029157; RRID: AB_10601020
Rabbit monoclonal anti-HOXB4	Abcam	Cat#ab133521; RRID: AB_2910615
Rabbit monoclonal anti-LMX1B	Abcam	Cat#ab259926; RRID:N/A
Rabbit polyclonal anti-BHLHB5	Invitrogen	Cat#PA5-64189; RRID:AB_2638547
Rabbit polyclonal anti-FOXP2	Abcam	Cat#ab16046; RRID: AB_2107107
Rabbit monoclonal anti-ISLET1	Abcam	Cat#ab109517; RRID:AB_10866454
Rabbit polyclonal anti-SIM1	OriGene	Cat#AP53918PU-N; RRID:N/A
Rabbit polyclonal anti-PAX2	Biolegend	Cat#901001; RRID: AB_2565001
Rabbit monoclonal anti-human MAP-2	Abcam	Cat#ab254263; RRID:N/A

(*Continued on next page*)

Continued

REAGENT or RESOURCE	SOURCE	IDENTIFIER
Rabbit polyclonal anti-Tuj-1	Abcam	Cat#ab18207; RRID:AB_444319
Rabbit polyclonal anti-NF200	Sigma-Aldrich	Cat#N4142; RRID:AB_477272
Rabbit polyclonal anti-MBP	Abcam	Cat#ab40390; RRID: AB_1141521
Rabbit polyclonal anti-GABA	Sigma-Aldrich	Cat#A2052; RRID:AB_477652
Rabbit polyclonal anti-Homer1	Synaptic System	Cat#160 003; RRID:AB_887730
Rabbit polyclonal anti-PKCγ	Abcam	Cat#ab71558; RRID: AB_1281066
Rabbit polyclonal anti-Calretinin	Swant	Cat#7697; RRID: AB_2619710
Rabbit polyclonal anti-Calbindin	Swant	Cat#CB38; RRID: AB_10000340
Rabbit polyclonal anti-NK1R	Sigma-Aldrich	Cat#S8305; RRID: AB_261562
Rabbit monoclonal anti-Parvalbumin	Abcam	Cat#ab181086; RRID: AB_2924658
Rabbit monoclonal anti-n-NOS	Abcam	Cat#ab76067; RRID: AB_2152469
Rabbit polyclonal anti-NPY	ImmunoStar	Cat#22940; RRID: AB_10720817
Rabbit monoclonal anti-RORβ	Abcam	Cat#ab187657; RRID:N/A
Rabbit polyclonal anti-NSE	Synaptic System	Cat#230 003; RRID: AB_10641163
Rabbit polyclonal anti-KCC2	Millipore	Cat#07-432; RRID: AB_310611
Rabbit polyclonal anti-TH	Novus	Cat#NB300-109; RRID:AB_10077691
Rabbit polyclonal anti-CGRP	Peninsula Lab	Cat#T-4032; RRID: AB_518147
Rabbit monoclonal anti-GAD65/67	Abcam	Cat#ab239372; RRID:N/A
Rabbit monoclonal anti-VGLUT2	Abcam	Cat#ab216463; RRID: AB_2893024
Rabbit monoclonal anti-GAP43	Millipore	Cat#AB5312; RRID:AB_2109488
Rabbit polyclonal anti-Laminin	Sigma-Aldrich	Cat#L9393; RRID:AB_477163
Rabbit monoclonal anti-Vimentin	Abcam	Cat#ab92547; RRID: AB_10562134
Rabbit monoclonal anti-GFAP	Cell Signaling Technology	Cat#12389; RRID: AB_2631098
Rabbit monoclonal anti-S100β	Abcam	Cat#ab52642; RRID: AB_882426
Rabbit monoclonal anti-ALDH1L1	Abcam	Cat#ab300509; RRID:N/A
Rabbit polyclonal anti-AQP4	Millipore	Cat#AB3594; RRID: AB_91530
Rabbit monoclonal anti-Connexin 43	Abcam	Cat#ab235585; RRID:N/A
Rabbit monoclonal anti-Ki67	Abcam	Cat#ab16667; RRID:AB_302459
Rabbit polyclonal anti-c-Caspase-3	Cell Signaling Technology	Cat#9661; RRID:AB_2341188
Rabbit monoclonal anti-OCT4	Abcam	Cat#ab181557; RRID:AB_2687916
Sheep polyclonal anti-ChX10	Millipore	Cat#AB9016; RRID: AB_2216009
Donkey anti chicken Cy3	Jackson ImmunoResearch	Cat#703-165-155; RRID:AB_2340363
Donkey anti mouse Alexa Fluor 488	Invitrogen	Cat#A-21202; RRID:AB_141607
Donkey anti mouse Alexa Fluor 647	Invitrogen	Cat#A-31571; RRID:AB_162542
Donkey anti rabbit Alexa Fluor 488	Invitrogen	Cat#A-21206; RRID:AB_2535792
Donkey anti rabbit Alexa Fluor 594	Invitrogen	Cat#A-21207; RRID:AB_141637
Donkey anti goat Alexa Fluor 488	Invitrogen	Cat#A-11055; RRID:AB_2534102
Donkey anti goat Alexa Fluor 594	Invitrogen	Cat#A-11058; RRID:AB_2534105
Donkey anti guinea pig Alexa Fluor 488	Jackson ImmunoResearch	Cat#706-545-148; RRID:AB_2340472
Donkey anti guinea pig Alexa Fluor 647	Jackson ImmunoResearch	Cat#706-605-148; RRID:AB_2340476
Donkey anti sheep Alexa Fluor 488	Invitrogen	Cat#A-11015; RRID: AB_141362
Chemicals, peptides, and recombinant proteins		
Optimal Cutting Temperature Compound	Sakura	4853
Hematoxylin Solution	Servicebio	G1004
Eosin Solution	Servicebio	G1001

(*Continued on next page*)

Continued

REAGENT or RESOURCE	SOURCE	IDENTIFIER
Quick Block Blocking Buffer	Beyotime	P0260
Quick Block Primary Antibody Dilution Buffer	Beyotime	P0262
Quick Block Secondary Antibody Dilution Buffer	Beyotime	P0265
Xylazine Hydrochloride	Sigma-Aldrich	X1251
Clozapine-N-Oxide	MedChemExpress	HY-17366
Salvinorin B	Cayman Chemical	23582
BDA Biotin 10000 WM	Invitrogen	D1956
Streptavidin Alexa Fluor 488	Invitrogen	S32354
Hoechst 33258	Sigma-Aldrich	94403
Critical commercial assays		
Zoletil 50	Virbac S.A., Carros, France	N/A
Prolong Glass Antifade Mount	Invitrogen	P36980
Experimental models: Cell lines		
hESCs Lines (line WA09)	Xiong et al.[55]	N/A
hM3Dq-KORD-expressing hESCs Lines (line WA09)	Xiong et al.[55]	N/A
Experimental models: Organisms/strains		
Rat: Crl:NIH-Foxn1rnu Nude Rat	Beijing Vital River Laboratory Animal Technology Co., Ltd	N/A
Software and algorithms		
TreadScan	Clever System	https://cleversysinc.com/CleverSysInc/csi_products/treadscan/
Fiji	NIH	https://fiji.sc RRID: SCR_002285
AngioTool	National Cancer Institute	https://ccrod.cancer.gov/confluence/display/ROB2/Home RRID: SCR_016393
Prism 8	GraphPad Software	https://www.graphpad.com RRID: SCR_002798
R Project	The R Project for Statistical Computing	https://www.r-project.org RRID: SCR_001905
Other		
Surgical Microscope	World Precision Instruments	PSMB5N
Small Animal Spinal Unit	David Kopf Instruments	Model 980
Small Animal Stereotaxic Unit	David Kopf Instruments	Model 902
RN Compression Fitting	Hamilton	55750-01
Gas Tight Syringe	Hamilton	7656-01
Glass Capillaries	World Precision Instruments	1B100F-4
UltraMicroPump	World Precision Instruments	UMP3T
Flaming/Brown Micropipette Puller	Sutter Instrument	P-97
Micro Grinder	Narishige	EG-402
Digital Video Camera	SONY	HDR-CX450
Electronic von Frey Anesthesiometer	IITC Life Sciences	2391
Hargreaves Method Plantar Test Apparatus	IITC Life Sciences	390
Gait Analysis Treadmill Exer Gait	Columbus Instruments	1008
Leica Cryostat	Leica Microsystems	CM1950
Confocal Laser Scanning Microscope	Olympus	FLUOVIEW FV3000

RESOURCE AVAILABILITY

Lead contact

Further information and requests for resources and reagents should be directed to and will be fulfilled by the lead contact, Wei Wang (wwang@tjh.tjmu.edu.cn).

Materials availability

This study did not generate new unique reagents.

Data and code availability

- All data reported in this paper will be shared by the lead contact upon request.
- This paper does not report original code.
- Any additional information required to reanalyze the data reported in this paper is available from the lead contact upon request.

EXPERIMENTAL MODEL AND STUDY PARTICIPANT DETAILS

Cells

The human ESC line (H9, WA09) and hM3Dq-KORD-expressing human ESC line (H9, WA09) (passages 20-40)[55] were cultured in a six-well plate covered with an irradiated mouse embryonic fibroblast (MEF) feeder layer. The hPSC medium consisted of modified Eagle's medium/nutrient mixture F-12 (DMEM/F-12), knockout serum replacement (KSR), 1x nonessential amino acid solution (NEAA), 0.5x GlutaMax-I supplement, 0.1 mM 2-mercaptoethanol, and 4 ng/ml FGF-2. The culture medium was changed daily, and the cells were passaged with Dispase II every week.

Animals

A total of 39 adult (8 weeks old) female athymic nude rats (Crl:NIH-Foxn1^{rnu}) purchased from Beijing Vital River Laboratory Animal Technology Co., Ltd. were the subjects of this study. After arrival, they were acclimated to the animal facility for at least 1 month before experiments were initiated. They were housed 2 rats per cage in an independent ventilation cage (IVC, 30 cm high, 27 cm wide, and 40 cm deep) with access to food and water *ad libitum* in a specific pathogen-free (SPF) housing room with a temperature maintained at 22°C-24°C, a relative humidity of 45-60%, and a 12-hour day/night cycle (lights on at 6:00 am and off at 18:00 pm). All animal experiments were performed under the protocol approved by the Committee on the Ethics of Animal Experiments and the Institutional Animal Care and Use Committee at Tongji Hospital, Tongji Medical College, Huazhong University of Science and Technology (ethics approval number, TJH-201903007).

METHOD DETAILS

Cell differentiation

Details regarding the differentiation of human ESCs into dorsal spinal dI4/dIL$_A$ GABA neurons were described in our recently published step-by-step protocol.[56] Briefly, human ESCs were cultured on MEFs, and in the presence of SB431542 (2 mM), DMH1 (2 mM) and CHIR99021 (3 mM) for 7 days, human ESCs were differentiated into SOX1-expressing neuroepithelia. In the presence of retinoic acid (RA, 0.1 mM) and cyclopamine (0.5 mM), a sonic hedgehog antagonist, from days 7-14, the neuroepithelia were differentiated into dorsal spinal progenitors. The progenitor cells were further differentiated into neurons on Matrigel-coated coverslips in neural basal medium with N2 supplement, B27 supplement, nonessential amino acid (NEAA), ascorbic acid (AA, 200 mM), cAMP (1 mM), brain-derived neurotrophic factor (BDNF, 10 ng/ml), and glial cell line-derived neurotrophic factor (GDNF, 10 ng/ml).

Cell transplantation

The details of transplanting cells into the rat cervical spinal cord were described previously.[57] Rats were anesthetized by intramuscular injection of tiletamine-zolazepam (Zoletil 50; Virbac S.A., Carros, France) (10 mg/kg), xylazine (2.5 mg/kg) and atropine (0.05 mg/kg). Both eyes were covered with eye ointment to prevent xerophthalmia. Ceftriaxone (50 mg/kg) was administered intraperitoneally for prophylaxis against infection. Body temperature was maintained at 37°C with a heating pad. After shaving the fur on the neck, the skin was disinfected with iodophor followed by alcohol. A midline incision was made, followed by blunt dissection of the para-spinal muscles. The laminae were exposed by a retractor, and the C5-C7 laminae were removed with a rongeur (RWD Life Science, 903-00321-00). The dura was slit longitudinally under a surgical microscope (World Precision Instruments, PBM). Rats were then mounted onto a small animal spinal unit (David Kopf Instruments, Model 980). Human dorsal spinal GABA NPCs were harvested and resuspended in culture medium at a density of 100,000 cells/μl. Through a 10 μl microsyringe (Hamilton, 7653-01), 2 μl of cell suspension was loaded into a beveled glass micropipette with a tip diameter of 40 μm made from a glass capillary (World Precision Instruments, 1B100F-4) through a Flaming/Brown Micropipette Puller (Sutter Instruments, PC-97) and a Micro Grinder (Narishige, EG-402). Then, the micropipette containing the cell suspension was connected to a 100 μl microsyringe (Hamilton, 7656-01) filled with saline through an RN compression fitting (Hamilton, 55750-01). Next, the microsyringe was mounted into a microinjection pump (World Precision Instruments, UMPT3) held by a stereotaxic manipulator. Under a surgical microscope, the micropipette was

placed 1 mm lateral to the midline and 1.5 mm deep to the dorsal surface of the C6 spinal cord, and the cells were slowly injected within 3 minutes. The pipette was left in place for 1 minute, followed by slow withdrawal. Using the same procedures, another 5 points in the C6-C8 spinal cord received the same volume of cell transplantation. Rats in the Medium group received intraspinal injection of the same volume of culture medium without cells. Another 3 rats received intraspinal transplantation of 200,000 human ESCs (in 2 μl medium) into the T10 spinal cord. The muscles, fascia, and skin were closed with interrupted sutures. Rats were subcutaneously injected with 5 ml of lactated Ringer's solution to prevent dehydration. Carprofen (10 mg/kg) was administered subcutaneously for 3 days to alleviate pain.

Mechanical allodynia

The mechanical withdrawal threshold was measured with an electronic Von Frey Anesthesiometer (IITC Life Sciences, 2391) as previously described.[58] Rats were placed in plexiglass chambers on a wire mesh floor in a quiet room for 30 min of acclimation starting 3 days before testing. On the day of testing, rats were allowed to acclimate for 30 min. A tilted mirror was placed under the mesh floor to provide a clear view of the fore and hind paws, which were stimulated at the center with a rigid tip (diameter 1 mm) attached to the recording apparatus. A gradual increase in pressure was applied until the withdrawal response appeared. Then, the stimulus was automatically discontinued, and the value was recorded and displayed by the device. The procedure was repeated three times with a minimum of 1 min interval between stimuli.

Thermal hyperalgesia

The thermal withdrawal latency was measured with a Hargreaves plantar test apparatus (IITC Life Sciences, 390) as previously described.[59] Rats were placed in plexiglass chambers on a glass stand in a quiet room for 30 min of acclimation starting 3 days before testing. On the day of testing, rats were allowed to acclimate for 30 min. A tilted mirror was placed under the mesh floor to provide a clear view of the fore and hind paws, which were stimulated at the center with a focused light spot. When the withdrawal response appeared, the light was turned off, and the latency was recorded. The cut off was set at 20 s, which means that if rats did not respond within 20 s, the light was turned off automatically to prevent harm, and the latency was recorded as 20 s. The procedure was repeated three times with a minimum of 1 min interval between stimuli.

Grooming test

Forelimb grooming function was assessed using a scoring system as previously described.[60] Cool tap water was applied to the animal's head and back with soft gauze, and the animal was returned to its home cage. Grooming activity was recorded with a video camera (SONY, HDR-CX450) from the onset of grooming through at least two stereotypical grooming sequences, which included licking of the forepaws and face washing, forelimb grooming of the face, repetitive licking of the body, and hind paw scratching. Slow motion video playback was used to score each forelimb independently by the maximal contact made while initiating any part of the grooming sequence.

Open field locomotion

Before testing, rats were allowed to acclimate to the open field two times per day for 5 days until they no longer showed signs of fear (crouching, cowering away from the examiner, little or no locomotion, frequent defecation and urination, piloerection, vocalizations, and failure to groom). During testing, rats were encouraged to continuously locomote. Hindlimb locomotion was evaluated using the Basso Beattie Bresnahan (BBB) Locomotor Rating Scale[61] during a 4 min observation period for each rat.

Horizontal ladder walking

The skilled locomotion of the fore and hind limbs was assessed with the horizontal ladder-walking test as previously described.[62] The horizontal ladder-walking test apparatus consisted of clear Plexiglas sidewalls (1 m in length) and unevenly spaced metal rungs (to prevent habituation) elevated approximately 30 cm from the ground. Before testing, rats were trained to cross the ladder three times per day for at least three days. During testing, a video camera (SONY, HDR-CX450) was positioned at a slight ventral angle so that both sides of the body and paw positions could be recorded simultaneously from a ventral view. Each experiment was performed in triplicate. The video recordings were analyzed using frame-by-frame analysis at 25 f/s. The average number of fore and hind limb misplacements while the rats walked through the 1 m long horizontal ladder was manually scored by an observer blinded to the groups. A complete miss, slip, or replacement of the paw during placement was considered an error. The average number of errors per trial was normalized to the average total number of steps per trial to obtain the results presented as a percentage of error. Then, the results were presented as a percentage of correct by percentage of error subtracted by 100%.

Gait analysis

Details of the methods were described previously.[63] Rats were allowed to quadrupedally walk on a transparent motor-driven treadmill belt at a speed of 15 cm/s for a period of 20 s to obtain at least ten consecutive step cycles of consistent walking for video analysis. Videos were imported into Tread Scan software to automatically analyze the gait parameters, as listed in Table S1. All the parameters were further analyzed with principal component analysis (PCA).[64] A total of 94 Tread Scan parameters were computed for each gait cycle. These parameters are detailed in Table S1. To compare the overall locomotion ability between groups, we performed a statistical analysis using PCA in R (v3.6.3). The 94 parameters for all rats together were included. Missing values were preprocessed through the mice R package (v3.13.0).

Component extraction and visualization were implemented using the R packages FactoMineR (v1.34) and factoextra (v1.0.7), respectively. Additionally, we applied the syndRomics package to help determine the most relevant components and generate illustrative results. The analyses were performed by investigators who were blinded to the treatment groups.

Chemogenetics

Twelve months after cell transplantation, the sensory and motor functions of rats were further evaluated when the activity of grafted cells was increased and inhibited with Bi-DREADDs. To activate human cells, 3 mg/kg clozapine-N-oxide (CNO, MCE, HY-190, 1 mg/ml in saline) was administered subcutaneously 30 min before behavior tests were initialized. To inhibit human cells, 10 mg/kg salvinorin B (SalB, Cayman Chemical, 20 mg/ml in DMSO) was administered subcutaneously 15 min before behavior tests were initialized.[65] As a control, a vehicle consisting of 2% DMSO in saline was also administered, and behaviors were tested. In addition, behaviors were also tested after the CNO, SalB and vehicle had been washed out from the rats.

Corticospinal tract tracing

Rats were anesthetized as described for cell transplantation. After shaving the fur on the scalp, the skin was disinfected with iodophor followed by alcohol. A midline incision was made to expose the cranium. Then, rats were mounted into a Small Animal Stereotaxic Unit (David Kopf Instruments, Model 902). Under a surgical microscope (World Precision Instruments, PBM), bilateral craniotomy was performed to expose the primary motor cortex (M1) and primary sensory cortex (S1) of the forelimb, and the dura was slit. Using a beveled glass micropipette and microinjection pump, 10% biotinylated dextran amine (BDA, WM 10 kDa, Invitrogen, D1956) was injected into six sites of M1 and S1 to label the corticospinal tract. The injection coordinates were as follows: anterior-posterior and medial-lateral coordinates from bregma in mm: 2.5/3, 2.5/4, 1.5/3, 1.5/4, 0.5/3, 0.5/4, depth 1.4 mm. The volume of each site was 0.5 μl. Four weeks after tracing, rats were perfused for histology.

Tissue processing

Rats received an intraperitoneal injection of 3 mg/kg CNO (MCE, HY-17366, 1 mg/ml in saline) to activate human neurons 2 hours before sacrifice. All rats were euthanized by intraperitoneal injection of sodium pentobarbital (60 mg/kg) and perfused through the heart with 500 ml heparinized (100,000 U/L) normal saline, followed by 500 ml 4% paraformaldehyde (PFA) in phosphate-buffered saline (PBS). The entire brains, spinal cords and other integral organs, including hearts, livers, spleens, lungs and kidneys, were harvested and postfixed in the same fixative at 4°C for 24 hours and then dehydrated in 300 ml of 30% sucrose solution at 4°C for 72 hours. Spinal cord segments comprising C5-T2 (for Medium, dI4, dI4-Bi-DREADDs) and T8-T12 (for hESCs) were dissected, embedded with optimum cutting temperature compound (Sakura, 4853), and flash frozen. Using a cryostat microtome (Leica, CM1950), serial horizontal sections 20 μm thick were cut, collected into cryoprotectant consisting of 30% sucrose and 30% ethylene glycol in PBS and stored at -80°C. Brains, integral organs and spinal cord segments of C1-C4 and T3-T6 were cut into serial coronal sections 40 μm thick. For histology analysis, 20 μm sections were cut and mounted onto slides.

Hematoxylin & eosin staining

Sections were dried at 37°C for 1 hour and washed 3 times with double distilled water for 10 minutes each. After air drying, the sections were immersed in hematoxylin solution (Servicebio, G1004) for 5 minutes, thoroughly rinsed with running tap water, differentiated in 75% ethanol containing 1% hydrochloric acid for 5 seconds, and immediately rinsed again with running tap water thoroughly. Finally, sections were stained in eosin solution (Servicebio, G1001) for 5 minutes, dehydrated 2 times with 100% ethanol for 5 minutes each, cleared 2 times in xylene for 5 minutes each, and cover-slipped with neutral balsam.

Immunofluorescence

Free-floating sections were washed 3 times with Tris-buffered saline containing 0.25% Triton-X-100 (TBST) for 5 minutes each, blocked with Quick Block ™ blocking buffer (Beyotime, P0260) for 15 minutes, and incubated overnight (more than 16 hours) with primary antibodies in Quick Block ™ primary antibody dilution buffer (Beyotime, P0262) at 4°C. Thereafter, the sections were rinsed 3 times again with TBST for 5 minutes each and then incubated with fluorochrome-conjugated secondary antibodies and Hoechst 33258 (Sigma, 94403) in Quick Block ™ secondary antibody dilution buffer (Beyotime, P0265) in the dark for 1 hour. Finally, the sections were washed 3 times with TBST for 5 minutes each, mounted onto slides, air dried thoroughly, and cover-slipped with Prolong Glass Antifade Mount (Invitrogen, P36980).

The following primary antibodies were used: chicken anti NeuN (Millipore, ABN91), goat anti-mCherry (biorbyt, orb11618), goat anti-OTX2 (R&D Systems, AF1979), goat anti-ChAT (Millipore, AB144P), goat anti-5-HT (ImmunoStar, 20079), goat anti-SOX9 (R&D Systems, AF3075), goat anti-OLIG2 (R&D Systems, AF2418), goat anti-SOX1 (R&D Systems, AF3369), goat anti-NANOG (R&D Systems, AF1997); guinea pig anti-NeuN (Millipore, ABN90), guinea pig anti-c-FOS (Synaptic System, 226003), guinea pig anti-VGAT (Synaptic Systems, 131004), guinea pig anti-Gephyrin (Synaptic Systems, 147318), guinea pig anti-rat VGLUT1 (Millipore, AB5905), guinea pig anti-GlyT2 (Synaptic Systems, 272004), guinea pig anti-DCX (Synaptic System, 326004), guinea pig anti-GLT-1 (Millipore, AB1783); mouse anti-human Nuclei (Millipore, MAB1281), mouse anti-PTF1A (Santa Cruz Biotechnology, sc-393011), mouse anti-BRN3A (Millipore, MAB1585), mouse anti human mitochondria (Millipore, MAB1273), mouse anti-STEM121 (Takara, Y40410), mouse anti-human Tau (BioLegend, 835201), mouse anti-HOXC8 (BioLegend, 920501), mouse anti-human Synaptophysin (Invitrogen, 14-6525-80), mouse anti-RECA1 (Bio-Rad, MCA970R), mouse anti-human GFAP (Takara, Y40420), mouse anti-human Nestin (R&D Systems, MAB1259); rabbit anti-mCherry (Abcam, ab167453), rabbit anti-HA (CST,

3724), rabbit anti-NeuN (Millipore, ABN78), rabbit anti-FOXG1 (Abcam, ab196868), rabbit anti-HOXA3 (Sigma, H3791), rabbit anti-HOXB4 (Abcam, ab133521), rabbit anti-PAX2 (Biolegend, 901001), rabbit anti-LMX1B (Abcam, ab259926), rabbit anti-BHLHB5 (Thermo, PA5-64189), rabbit anti-FOXP2 (Abcam, ab16046), rabbit anti-ISLET1 (Abcam, ab109517), rabbit anti-SIM1 (Origene, AP53918PU-N), rabbit anti-GABA (Sigma–Aldrich, A2052), rabbit anti-Calbindin (Swant, CB-38a), rabbit anti-Parvalbumin (Abcam, ab181086), rabbit anti-n-NOS (Abcam, ab76067), rabbit anti-NPY (Abcam, ab221145), rabbit anti-RORβ (Abcam, ab187657), rabbit anti-NSE (Synaptic System, 230003), rabbit anti-KCC2 (Millipore, 07-432), rabbit anti-CaMKIIα (Abcam, ab92332), rabbit anti-TH (Novus, NB300-109), rabbit anti-human MAP-2 (Abcam, ab254263), rabbit anti-Tuj-1 (Abcam, ab18207), rabbit anti-Neurofilament 200 kDa (Sigma, N4142), rabbit anti-GAP43 (Millipore, AB5312), rabbit anti-MBP (Abcam, ab40390), rabbit anti-Homer1 (Synaptic System, 160003), rabbit anti-GAD65/67 (Abcam, ab183999), rabbit anti-rat VGLUT2 (Abcam, ab239372), rabbit anti-PKCγ (Abcam, ab71558), rabbit anti-Calretinin (Swant, 7697), rabbit anti-NK1R (Sigma, S8305), rabbit anti-CGRP (Peninsula Lab, T-4032), rabbit anti-laminin (Sigma–Aldrich, L9393), rabbit anti-vimentin (Abcam, ab92547), rabbit anti-GFAP (Cell Signaling Technology, 12389), rabbit anti-S100β (Abcam, ab52642), rabbit anti-ALDH1L1 (Abcam, ab300509), rabbit anti-connexin 43 (Abcam, ab235585), rabbit anti-AQP4 (Millipore, AB3594), rabbit anti-NG2 (Millipore, AB5320), rabbit anti-Ki67 (Abcam, ab16667), rabbit anti-c-Caspase-3 (Cell Signaling Technology, 9661), rabbit anti-OCT4 (Abcam, ab181557), sheep anti-CHX10 (Millipore, AB9016).

The following secondary antibodies were used: donkey anti-mouse Alexa Fluor 488 (Invitrogen, A-21202), donkey anti-mouse Alexa Fluor 647 (Invitrogen, A-31571), donkey anti-rabbit Alexa Fluor 488 (Invitrogen, A-21206), donkey anti-rabbit Alexa Fluor 594 (Invitrogen, A-21207), donkey anti-goat Alexa Fluor 488 (Invitrogen, A-11055), donkey anti-goat Alexa Fluor 594 (Invitrogen, A-11058), donkey anti-guinea pig Alexa Fluor 488 (Jackson ImmunoResearch, 706-545-148), and donkey anti-guinea pig Alexa Fluor 647 (Jackson ImmunoResearch, 706-605-148).

Laser scanning confocal microscopy

Epifluorescence images were acquired using an Olympus FLUOR VIEW FV3000 confocal microscope. To avoid bleeding between channels, Hoechst 33258 and Cy3 were grouped into phase 1, Alexa Fluor 488 and Alexa Fluor 594 were grouped into phase 2, and Alexa Fluor 647 was set into phase 3. The bandwidth of each channel was set as follows: Hoechst 33258, 430-470 nm, Alexa Fluor 488, 500-540 nm, Cy3, 570-580 nm, Alexa Fluor 594, 610-630 nm, Alexa Fluor 647, and 650-750 nm. HV was set at 700, gain was set at 1, and offset was set at 10 for all channels. Under the Hi-Lo viewing mode, the laser intensity of each channel was adjusted to the maximum possible to avoid photobleaching and overexposure. The scanning speed was set at 8 μs/pixel. To capture the entire horizontal spinal cord section, multiple area time lapse imaging was employed. The matrix was set to 5*10 areas in rows and columns, and each area was acquired under a 10x objective lens with optical zoom set at 1 and resolution set at 256*256 pixels. For the region of interest, z stacks of images were captured under a 20x or 100x objective lens, with optical zoom set at 1-5 as needed and resolution set at 1024*1024. Images were postprocessed and analyzed with Fiji.[66] Analysis of RECA1$^+$ capillaries was performed with AngioTool.[67]

QUANTIFICATION AND STATISTICAL ANALYSIS

No statistics were used to determine strategies for randomization, sample size estimation, and inclusion and exclusion of any data. All data are represented as the mean ± SEM unless otherwise stated. All statistical analyses were performed using GraphPad Prism 8 with the exception of PCA using R. The Kolmogorov–Smirnov test was used to determine data normality. Statistics used for results analysis were as follows: unpaired Student's t test with Welch's correction for Figures 1B–1D, 2D and 3D, 3E, 4H, S1B–S1G, and S4F and S4G; one-way analysis of variance (ANOVA) followed by Tukey's test for Figures S4J–S4P; two-way repeated ANOVA followed by Tukey's test for Figures 3B and 3C, and mixed-effects models followed by Tukey's test for Figures 4A–4E, 4I–4K, and S4I. Differences were considered significant at $p < 0.05$ (*$p < 0.05$, **$p < 0.01$, and ***$p < 0.001$).